First Early Permian Paleomagnetic Pole for the Yili Block and its Implications for Late Paleozoic Postorogenic Kinematic Evolution of the SW Central Asian Orogenic Belt

Xin Zhu, Bo Wang, Yan Chen, Hongsheng Liu, Chorng-Shern Horng, Flavien Choulet, Michel Faure, Liangshu Shu, Zhenhua Xue

Tectonics

RESEARCH ARTICLE
10.1029/2017TC004642

Key Points:
- The first Early Permian paleomagnetic pole for the Yili Block is provided
- New quantitative constraints on late Paleozoic kinematic evolution of the SW Central Asian Orogenic Belt (CAOB) are made
- The large-scale strike slip movements played an important role in the tectonic evolution of the SW CAOB since the Permian

Supporting Information:
- Supporting Information S1
- Table S1
- Table S2

Correspondence to:
B. Wang,
bwang@nju.edu.cn;
burh_cw@yahoo.com

Citation:
Zhu, X., Wang, B., Chen, Y., Liu, H., Horng, C.-s., Choulet, F., et al. (2018). First Early Permian paleomagnetic pole for the Yili Block and its implications for late Paleozoic postorogenic kinematic evolution of the SW Central Asian Orogenic Belt. *Tectonics*, *37*, 1709–1732. https://doi.org/10.1029/2017TC004642

Received 27 APR 2017
Accepted 9 MAY 2018
Accepted article online 21 MAY 2018
Published online 5 JUN 2018

First Early Permian Paleomagnetic Pole for the Yili Block and its Implications for Late Paleozoic Postorogenic Kinematic Evolution of the SW Central Asian Orogenic Belt

Xin Zhu[1], Bo Wang[1], Yan Chen[2], Hongsheng Liu[1,2], Chorng-shern Horng[3], Flavien Choulet[4], Michel Faure[2], Liangshu Shu[1], and Zhenhua Xue[5]

[1]State Key Laboratory for Mineral Deposits Research, School of Earth Sciences and Engineering, Nanjing University, Nanjing, China, [2]Institut des Sciences de la Terre d'Orléans, UMR 7327, CNRS-Université d'Orléans, Orléans, France, [3]Institute of Earth Sciences, Academia Sinica, Taipei, China, [4]Chrono-Environnement, UMR 6249, CNRS-Université de Bourgogne Franche-Comté, Besançon, France, [5]Institute of Geology and Geophysics, Chinese Academy of Sciences, Beijing, China

Abstract We conducted a paleomagnetic study on the Early Permian volcanic and sedimentary rocks, and the Neoproterozoic mafic dikes in the Yili Block, NW China. Magnetite and hematite were proven to be the principal magnetic remanence carriers. Demagnetizations revealed stable characteristic remanence magnetizations with a sole reversed magnetic polarity. The magnetic remanence of only the Early Permian strata turned out to be primary based on positive fold tests; meanwhile, the magnetic remanence age of the mafic dikes is ambiguous. Accordingly, the first Early Permian paleomagnetic pole for the Yili Block is calculated at $\lambda = 81.5°$N, $\varphi = 256.5°$E, $N = 11$, and $A_{95} = 10.9°$. Comparisons of this new pole with published ones from the Yili, Tarim, and South Junggar blocks provide new quantitative constraints on late Paleozoic kinematic evolution of the SW Central Asian Orogenic Belt: (1) Between the Yili and Tarim blocks, significant relative movement took place along major strike-slip faults during the Late Carboniferous to Early Permian (580 ± 290 km) and the Early to Late Permian (585 ± 340 km), and the displacement rate increased from the Late Carboniferous to Early Permian (~19.3 ± 9.7 mm/yr) to the Early to Late Permian (~29.3 ± 17.0 mm/yr); (2) a significant relative rotation of 28.3° ± 18.3° in the Late Permian, and a lateral displacement of 630 ± 295 km after the Late Permian occurred between the Yili and South Junggar blocks. The significant strike-slip movements played an important role in the formation of the Central Asian Orogenic Belt and should be considered with great attention in tectonic and paleogeographic reconstructions.

1. Introduction

The Central Asian Orogenic Belt (CAOB; Figure 1a; Jahn et al., 2000; Jahn, 2004) or the Altaïds (Sengör et al., 1993), extending more than 4,000 km from the Urals to the Pacific Ocean, is located between the Siberia Craton to the north and the Karakorum, Tarim, and North China cratons to the south (Jahn, 2004; Windley et al., 2007). It is one of the largest accretionary orogens in the world (Dobretsov et al., 2003; Gao et al., 1998, 2009, 2011; Mossakovsky et al., 1994; Safonova et al., 2011; Shu et al., 2002; Wang et al., 2008; Wang, Jahn, et al., 2011; Wang, Liu, et al., 2014; Wang, Shu, et al., 2011, 2014; Wilhem et al., 2012; Xiao et al., 2004, 2008). Due to its long and complicated evolution and significant growth of continental crust, the CAOB has become one of the most attractive subjects of research in the geoscience community since the last three decades. On the contrary to the early models that suggested a continuous subduction and accretion of oceanic components forming a single long-living volcanic arc system (Sengör et al., 1993; Sengör & Natal'in, 1996), it is now well accepted that the CAOB formed through successive accretion and amalgamation of various microcontinents, arc complexes, and accretionary wedges during the closure of the Paleo-Asian Ocean (e.g., Eizenhöfer et al., 2014; Geng et al., 2011; Jiang et al., 2012; Levashova et al., 2009; Wong et al., 2010; Xiao et al., 2010, 2013; Yin et al., 2010).

However, several basic questions are still intensively debated and need further studies, some of which are listed below. (1) Which are the tectonic affinities and paleogeographic relationships of the microcontinents with Precambrian basements? The overall stratigraphic similarities between the Late Neoproterozoic and Cambrian series exposed on several continental blocks in the CAOB (e.g., Ankinovitch, 1962; Figure 1b) were variously interpreted. It has been suggested that these continental blocks drifted either from East Gondwana in the Neoproterozoic (Kheraskova et al., 2003), Siberia in the Late Neoproterozoic (Berzin & Dobretsov, 1993),

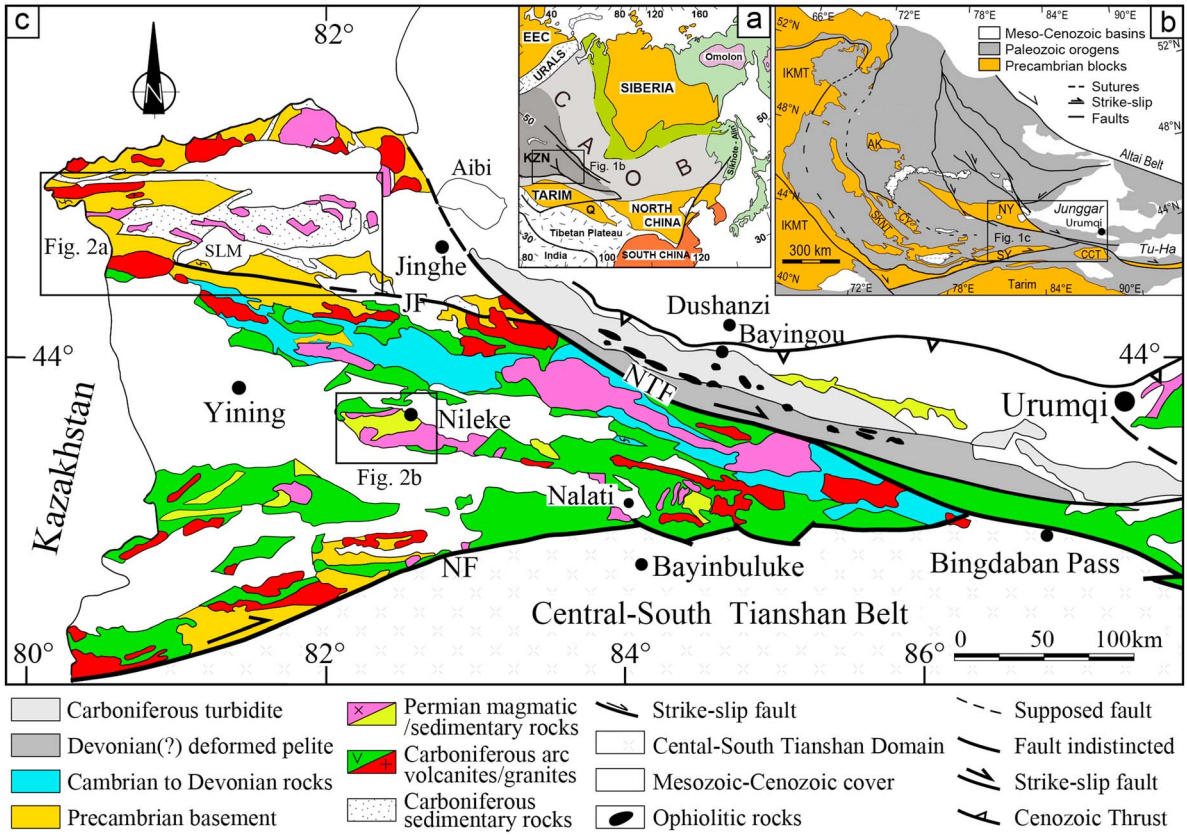

Figure 1. (a) Simplified tectonic divisions of the eastern Asia showing the location of the Central Asian Orogenic Belt (CAOB) and its surrounding blocks (after Jahn, 2004; Wang, Liu, et al., 2014). EEC = East European Craton; KZN = Kazakhstan; Q = Qaidam. (b) Sketch map of the southwestern part of the CAOB showing the distribution of main microcontinents and accretionary belts. Abbreviations: AK = Aktau, CCT = Chinese Central Tianshan, CY = Chu-Yili, IKMT = Ishim-Kyrgyz Middle Tianshan, NY = North Yili, SKNT = Stepnyak-Kyrgyz North Tianshan, SY = South Yili. (c) Simplified geological map of the Yili Block (modified after XBGMR, 1988a, 1988b). Abbreviations: NTF = North Tianshan Fault, NF = Nalati Fault, JF = Jinghe Fault.

Siberia or Baltica in the Ediacaran (Sengör & Natal'in, 1996), or from the Tarim and/or South China blocks (Levashova et al., 2011). (2) Which is the timing of the final amalgamation of the CAOB? Numerous studies have been conducted to understand the time-space pattern of these accretionary orogens (e.g., Charvet et al., 2011; Choulet et al., 2012, 2013; Gao et al., 1998, 2011; Han et al., 2011; Shu et al., 2004, 2011; Wang et al., 2008, 2010; Xiao et al., 2004, 2008, 2013); however, no consensus is achieved up to now. For example, oceanic basins were suggested to exist in the South Tianshan until the end-Permian on the basis of radiolarian fossils found in siliceous rocks of the South Tianshan mélange (Li et al., 2002, 2005), but many others argued that the oceanic basins within the Tianshan Orogen closed at the end of the Late Carboniferous (Allen et al., 1992; Gao et al., 1998; Han et al., 2011; Wang et al., 2006, 2008, 2010, 2018; Wang, Shu, et al., 2011). (3) How well constrained is the kinematics of the intracontinental movements? Wang, Chen, et al. (2007) regarded the Yili and Junggar blocks in the southwestern part of the CAOB as a welded block since the Late Carboniferous; thereafter, the study of Choulet et al. (2011) implied that the Junggar Block was not yet a rigid block until the end of the Paleozoic.

The late Paleozoic is a key period for studying the amalgamation and the postorogenic intracontinental tectonics of the CAOB (e.g., Choulet et al., 2011, 2013; Wang, Chen, et al., 2007; Xiao et al., 2015). As the southernmost part of the CAOB, the Tianshan Orogen played a major role in the agglomeration and subsequent intracontinental evolution of the CAOB. Hence, the relative movements of the three continental blocks in this region (Yili, South Junggar, and Tarim) in late Paleozoic will provide important constraints on the kinematic history of the SW CAOB. Accordingly, we conducted a paleomagnetic study on the Early Permian volcanic and sedimentary rocks and the Neoproterozoic mafic dikes from the Yili Block.

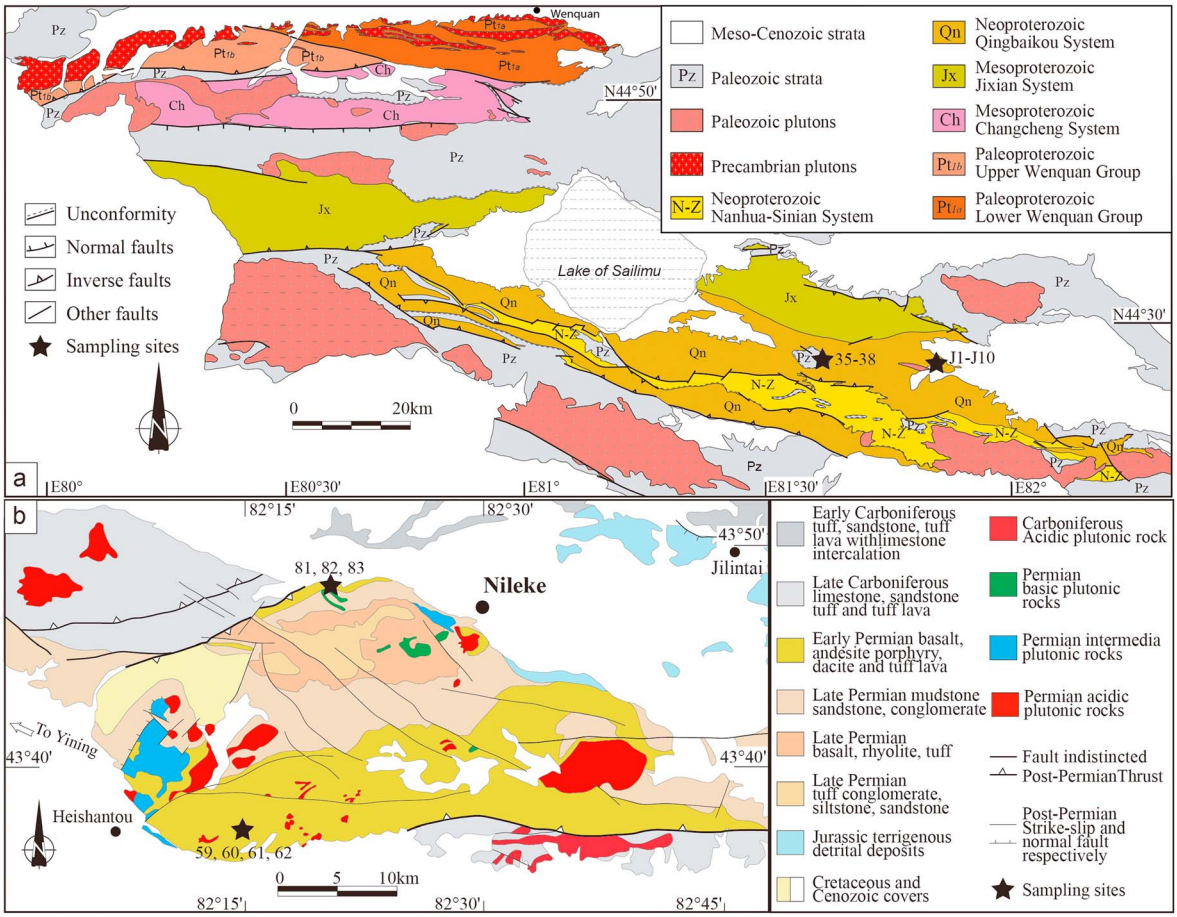

Figure 2. Simplified geological maps of the sampling areas: (a) the northern part of the Yili Block (Jinghe area) where sites J1-J10 and 35–38 were sampled; (b) the central part of the Yili Block (Nileke area) where sites 59–62 and 81–83 were sampled.

2. Geological Setting and Sampling

2.1. Geological Setting

In the CAOB, several microcontinents with Precambrian basement are separated by various Paleozoic accretionary complexes (Kröner et al., 2007; Windley et al., 2007; Xiao et al., 2004, 2010). The Yili Block (Figure 1b; Wang et al., 2008) is one of these microcontinents (Gao et al., 1998; Wang, Liu, et al., 2014; Wang, Shu, et al., 2014) and presents a triangular area in NW China extending westward into eastern Kazakhstan (Figures 1a and 1b). It is bordered to the north by the North Tianshan Fault (NTF) in the Chinese North Tianshan, which is a late Paleozoic accretionary complex, and to the south by the Nalati Fault in the Chinese Central Tianshan, which is an early Paleozoic continental arc with a Precambrian basement (Wang et al., 2010, 2018). The NTF and Nalati Fault are two Permian large-scale strike-slip faults that reworked the earlier suture zones (Charvet et al., 2011; Laurent-Charvet et al., 2002, 2003; Wang et al., 2006, 2009).

The Precambrian basement of the Yili Block is mainly exposed along its northern and southern margins; its central part is covered by thick Mesozoic to Cenozoic sedimentary sequences (XBGMR, 1993; Figure 1c). The Precambrian basement is mainly composed of Meso- to Neoproterozoic carbonates and amphibolite facies metasedimentary and meta-igneous rocks (Chen et al., 2000; Hu et al., 2010; Liu et al., 2014; Wang, Liu, et al., 2014; Wang, Shu, et al., 2014; XBGMR, 1993). Early Paleozoic rocks consist of Cambrian to Ordovician carbonates and clastic rocks and Silurian flysch in the north of the Yining area (XBGMR, 1993; Wang, Liu, et al., 2014; Wang, Shu, et al., 2014; Figures 1 and 2a). Late Paleozoic rocks include Devonian terrigenous rocks and arc-type granitoids, Carboniferous sandstones, limestones intercalated with pyroclastic rocks, volcanic rocks, and coeval granitoids. Permian formations consist of conglomerates and terrestrial

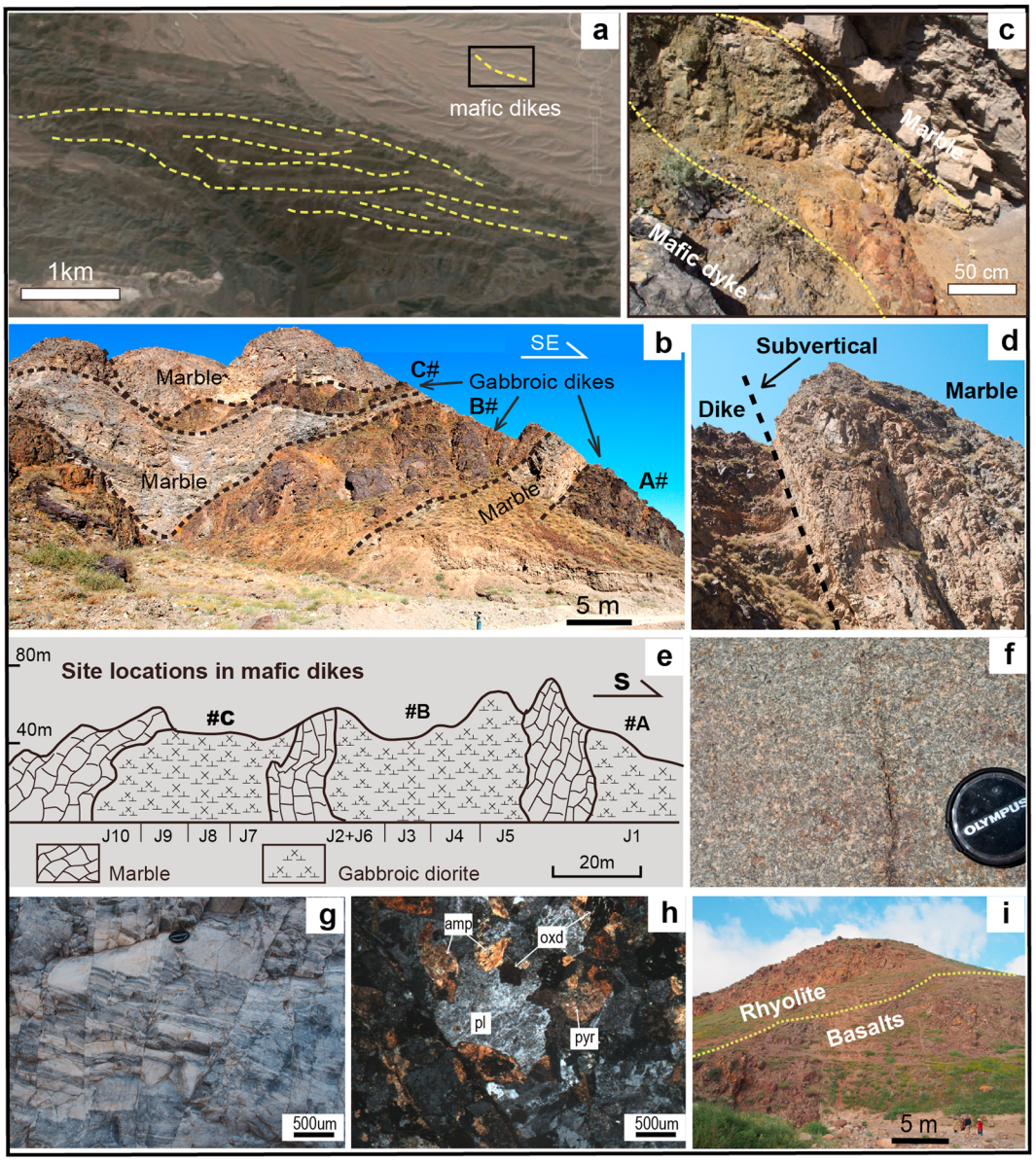

Figure 3. (a) Satellite image showing several tens of ESW-WNW-extending mafic dikes intruding the Neoproterozoic meta-carbonates; (b) panorama of three mafic dikes and the host marbles; (c) contact zone between the mafic dike and the host meta-carbonate, a >50-cm-wide interaction zone is characterized by skarnization, cataclastic deformation, and intense secondary alteration; (d) the contact relationship between mafic dikes and host marble suggesting a nearly vertical intrusion; (e) sketch of the Neoproterozoic dikes showing the locations of sampling sites; (f) a coarse-grained texture of gabbroic diorite dike; (g) intensively deformed marbles of the Proterozoic Kairtas Group; (h) photomicrograph of a gabbroic diorite which is composed of subhedral to euhedral amphiboles (amp), pyroxenes (pyr), plagioclases (pl), and minor oxides (oxd); (i) field photograph of basalts sampled from the Nileke area.

sandstones unconformably overlying the older rocks, with widespread Early Permian volcanic and plutonic rocks (Wang et al., 2009; XBGMR, 1993).

In the northern part of the Yili Block, Precambrian rocks exposed around the Sailimu Lake (SW of the Jinghe area) are mainly composed of (1) micaschists, paragneisses, amphibolites, quartzites, migmatites, orthogneisses, and gneissic granites belonging to the Wenquan Metamorphic Complex (XBGMR, 1993; Hu et al., 2006, 2010; Liu et al., 2014; Wang et al., 2012; Wang, Liu, et al., 2014; Wang, Shu, et al., 2014; Figures 1 and 2a); (2) intensively deformed crystalline limestones and interlayered phyllites of the Jixian System; (3)

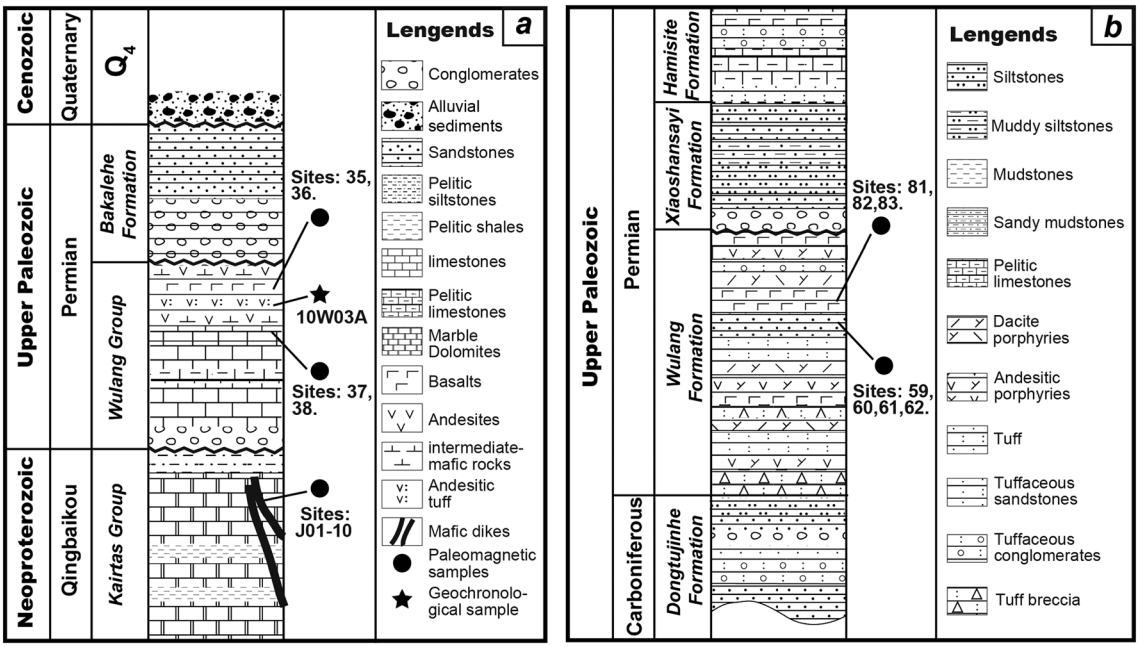

Figure 4. Synthetic stratigraphic columns of the sampling areas: (a) the northern part of the Yili Block (the Jinghe area); (b) the central part of the Yili Block (the Nileke area). The solid circles represent the stratigraphic positions of the paleomagnetic samples, and the solid star stands for the position of the geochronological sample (10W03A).

stromatolite-bearing dolomitic limestones and marbles of the Qingbaikou System; and (4) nonmetamorphic and undeformed sandstones, limestones, and interlayered diamictites belonging to the Nanhua and Sinian Systems (Ding et al., 2009; XBGMR, 1993). These Precambrian rocks are unconformably overlain by Cambrian phosphorous sandstones, phosphorites, limestones, mudstones and banded cherts changing upward to Ordovician-Silurian pelitic limestones, cherts, mudstones, and black shales (Figure 2a; XBGMR, 1988a, 1988b, 1993).

A group of Neoproterozoic (778–776 Ma; Wang, Liu, et al., 2014) mafic dikes crosscut the carbonates of the Kairtas Group (Qingbaikou System) on the eastern side of the Sailimu Lake (Figure 2a; XMBGR, 1988b). The mafic dikes are generally subvertical and show an overall ESE-WNW strike with widths varying from ~30 cm to several tens of meters (Figures 2a and 3a–3d). Chilled margins of the dikes and silicification of the host rocks can be observed to confirm an intrusive contact. A fine-grained texture is often observed in thin dikes and in the marginal facies of the thicker ones, and a coarse-grained texture is commonly present in the inner part of thick dikes. All dikes are composed of variable contents of pyroxene and plagioclase with a subordinate amount of amphibole (Figures 3f and 3h); thus, they belong to gabbros or gabbroic diorites. The intrusion-related thermal aureole is generally more than 50 cm wide (Figure 3c). The host rocks consist of argillites, black and white marbles, pelitic limestones, and interlayers of carbonaceous shales (Figure 3g). These rocks were intensively deformed, showing tight folds with subvertical bedding and steeply plunging fold axis (Figures 3b, 3d, and 3g). In contrast, no obvious deformation can be recognized in the mafic dikes.

About 10 km to the west of the mafic dikes along the Kusongmuqieke River, a sequence of volcanic and sedimentary rocks crops out in an area about 10 km^2 (Figure 2a). From bottom to top, the sequence is composed of the Lower Permian Wulang Group and the Bakalehe Formation. These Permian strata unconformably overlie the Neoproterozoic Kairtas Group (Figure 4a). The Wulang Group consists of calcareous conglomerates, basalts, andesitic basalts, and limestones. The vesicular and amygdaloidal structures can be recognized in basalts and andesitic basalts. The Bakalehe Formation is composed of conglomerates, gray sandstones, and red sandstones unconformably overlying the Wulang Group (Figure 4a).

In the Nileke area, central part of the Yili Block, late Paleozoic volcanic and sedimentary rocks are widely exposed (Figure 2b). The volcanic and sedimentary sequences can be divided into the Dongtujinhe,

Wulang, Xiaoshansayi, Hamisite, Tiemulike, and Kashihe Formations (Figure 4b). Among them, the Lower Permian Wulang Formation is composed of, from bottom to top, (1) gray tuffaceous sandstones, andesitic porphyries, and dacite porphyries with tuff breccia; (2) amygdaloidal basalts, sandstones, tuffaceous sandstones, dacite porphyries, amygdaloidal andesitic porphyries, and tuff breccia; and (3) basalts, andesitic porphyries with tuffaceous conglomerates, volcanic breccia, and dacite porphyries (Figure 4b).

2.2. Paleomagnetic and Geochronological Sampling

Tens of mafic dikes can be recognized from satellite images (Figure 3a); however, only few of them are accessible due to highly variable topography and very poor road conditions. Eighty-four cores were sampled for paleomagnetic study from 3 thick dikes, namely, A# (15 m thick, 1 site), B# (42 m thick, 5 sites), and C# (30 m thick, 4 sites; Figure 3b). These samples were evenly distributed in the dikes, from the chilled margin to the central part (Figure 3e). In addition, 40 cores from 4 sites were collected from the Lower Permian volcanic and sedimentary sequences of the Wulang group in the Jinghe area. Two sites were located in the basalts and the other two in the carbonates. An andesitic tuff sample (10W03A) interlayered in the amygdaloidal basalts and andesitic basalts was also collected for geochronological analysis (Figure 4a). Furthermore, 43 cores were sampled from 3 sites of sandstones and 4 sites of basalts in the Lower Permian Wulang Formation of the Nileke area (Figures 3i and 4b).

More than six cores were sampled from each site with a portable gasoline drill, and each core was oriented by magnetic and also by solar compasses whenever possible. The average difference between these two azimuth readings was calculated at 4.2° ± 1.8°, which is used to correct the orientation of samples measured only by magnetic compass. A complete sample list and more details are presented in Table 1.

3. Laboratory Analytic Methods

Core samples were first cut into standard cylindrical specimens, that is, 2.5 cm in diameter and 2.2 cm in length, for the measurements of magnetic remanence and acquisition of isothermal remanent magnetization (IRM). The rock powders were made from representative cores for thermal magnetic and hysteresis curve experiments. Thin sections were prepared for microscopic observations to identify mineral compositions and deformation features of the samples.

3.1. Magnetic Mineralogical Investigations

In order to identify the carriers of the magnetic remanence and susceptibility, representative samples were chosen for several magnetic mineralogical experiments. The acquisition of IRM was conducted with an ASC IM-10-30 impulse magnetizer and a JR-6A spinner magnetometer. Thermomagnetic experiments were carried out using a KLY-3S kappa bridge susceptibility meter coupled with a CS-3 furnace. These experiments were carried out in the Paleomagnetic Laboratory of the State Key Laboratory for Mineral Deposits Research (SKLMDR, Nanjing University). The magnetic hysteretic curves were acquired with a QUEL instrument in Laboratoire du Paléomagnétisme of Institut de Physique du Globe de Paris.

3.2. Magnetic Remanence Measurement and Directional Analysis

At least six specimens were selected from each site for demagnetization which was conducted at the Paleomagnetic Laboratory of SKLMDR (Nanjing), Institute of Earth Environment, Chinese Academy of Sciences (Xi'an), and the Institute of Earth Sciences, Academia Sinica (Taipei). Both progressive thermal and alternating field (AF) demagnetization procedures were used to clean the magnetic remanence of specimens. About 12 steps with a 50°C increment from room temperature to 500°C and a 30°C increment from 500°C to 690°C were applied for thermal demagnetization. The AF demagnetization was conducted in about 10 steps up to 100 mT with intervals varying from 5 to 20 mT. Magnetic components in the majority of specimens were determined with thermal demagnetization.

Remanence of specimens was measured with a JR-6A spinner magnetometer and a 2G Enterprises Inc. cryogenic rock magnetometer (2G-755) housed in a magnetically shield room. Demagnetization results were plotted on orthogonal vector diagrams (Zijderveld, 1967). Visually identified linear trajectories were used to determine directions of magnetic components by principal component analysis, employing a least-square fit comprising three or more demagnetization steps (Kirschvink, 1980), anchoring the fitting lines to the origin where appropriate. Site-mean directions were computed using the principal component

Tectonics

10.1029/2017TC004642

Table 1

Paleomagnetic Sampling and Analytical Results From the Early Permian Volcanic and Sedimentary Rocks and Neoproterozoic Mafic Dikes of the Yili Block

Section	Site	Lithology	S-Lat (N°)	S-Long (E°)	Strike (°)	Dip (°)	n/n_o (N)	D_g (°)	I_g (°)	D_s (°)	I_s (°)	k	α_{95} (°)	Pole Lat_g (N°)	Pole $Long_g$ (E°)	A_{95g} (°)	Pole Lat_s (N°)	Pole $Long_s$ (E°)	A_{95s} (°)
Volcanic and sedimentary rocks																			
Jinghe	35	Basalt	44°26′57.4″	81°36′27.5″	208	35	6/9	245.1	−59.7	176.7	−61.9	46.2	11.4	43.1	152.4	14.9	87.3	323.6	15.6
	36						6/9	260.5	−47.9	209.4	−65.9	28.5	14.6	26.3	155.8	15.4	69.5	150.8	21.5
	37	Limestone	44°26′56.2″	81°37′4.6″	232	48	6/11	262.4	−50.9	198.2	−49.1	72.9	7.9	26.6	152.4	8.8	69.6	210.7	8.5
	38						6/11	275.5	−66.6	172.1	−54.8	68.0	8.2	29.0	129.8	12.2	79.0	297.7	9.8
Nileke	59	Basalt	43°37′13.4″	82°13′53.6″	229	23	5/5	227.4	−49.1	204.9	−40.1	7.7	29.4	50.3	175.9	31.6	60.9	209.4	27.5
	60	Sandstone	43°38′36.1″	82°14′53.6″	45	40	6/6	163.7	−25.8	186.1	−59.4	98.3	6.8	56.9	292.2	5.4	84.3	207.2	8.9
	61						6/6	152.8	−23.4	165.6	−61.5	55.1	9.1	50.8	307.2	7.1	79.5	351.9	12.3
	62						3/6	148.0	−34.4	164.5	−73.2	83.0	13.6	53.6	319.8	11.8	72.0	55.6	23.0
	81	Basalt	43°48′4.4″	82°21′14.0″	85	49	7/7	180.3	14.7	180.5	−34.3	70.2	7.3	38.7	262.0	5.3	65.0	261.2	6.3
	82						7/7	168.3	5.4	164.3	−42.4	69.8	7.3	42.3	278.2	5.2	66.9	301.1	7.0
	83						6/6	168.5	20.6	167.9	−27.6	63.0	8.5	34.6	276.1	6.5	59.1	285.5	6.9
$Mean_{11}$							11	190.2	−39.2			3.0	32.1	67.2	218.9	31.6			
							11			181.1	−53.2	22.1	9.9				81.5	256.5	10.9
Mafic dikes																			
A#	J1	Gabbroic diorite	44°26′23.4″	81°51′45.7″			9/9	179.9	−48.4			58.9	6.8	74.9	262.2	7.2			
B#	J2		44°26′25.9″	81°51′47.5″			10/10	199.2	−62.1			41.5	7.6	76.2	169.5	10.4			
	J3						6/8	199.5	−51.6			23.8	14.0	70.5	203.9	15.8			
	J4						8/8	186.4	−55.6			26.6	10.9	80.4	229.2	13.2			
	J5						9/9	205.6	−55.6			42.1	8.0	68.9	186.1	9.7			
	J6						8/8	174.7	−62.5			49.4	8.0	86.2	345.4	11.1			
C#	J7		44°26′31.4″	81°51′44.2″			8/8	211.9	−46.6			25.6	11.2	59.7	194.2	11.6			
	J8						8/8	183.1	−52.7			38.2	9.1	78.6	248.7	10.5			
	J9						8/8	191.7	−50.5			35.0	9.5	74.0	223.0	10.5			
	J10						6/8	176.3	−62.0			35.9	11.3	87.1	329.7	15.4			
$Mean_{10}$							10	191.5	−55.3			74.8	5.6	78.3	211.8	7.2			

Notes. Abbreviations: S-Lat (N°)/S-Long (E°), latitude and longitude of sampling sites. *n/no* (*N*), number of specimens in calculation/totally sampled (sites). D_g, I_g, D_s, and I_s, declination (D) and inclination (I) in geographic (g) and stratigraphic (s) coordinates. *k*, precision parameter; $\alpha 95$, 95% confidence interval. Lat_g, $Long_g$, Lat_s, $Long_s$, and A95, latitude and longitude of paleomagnetic poles in geographic (g) and stratigraphic (s) coordinates, and 95% confidence interval.

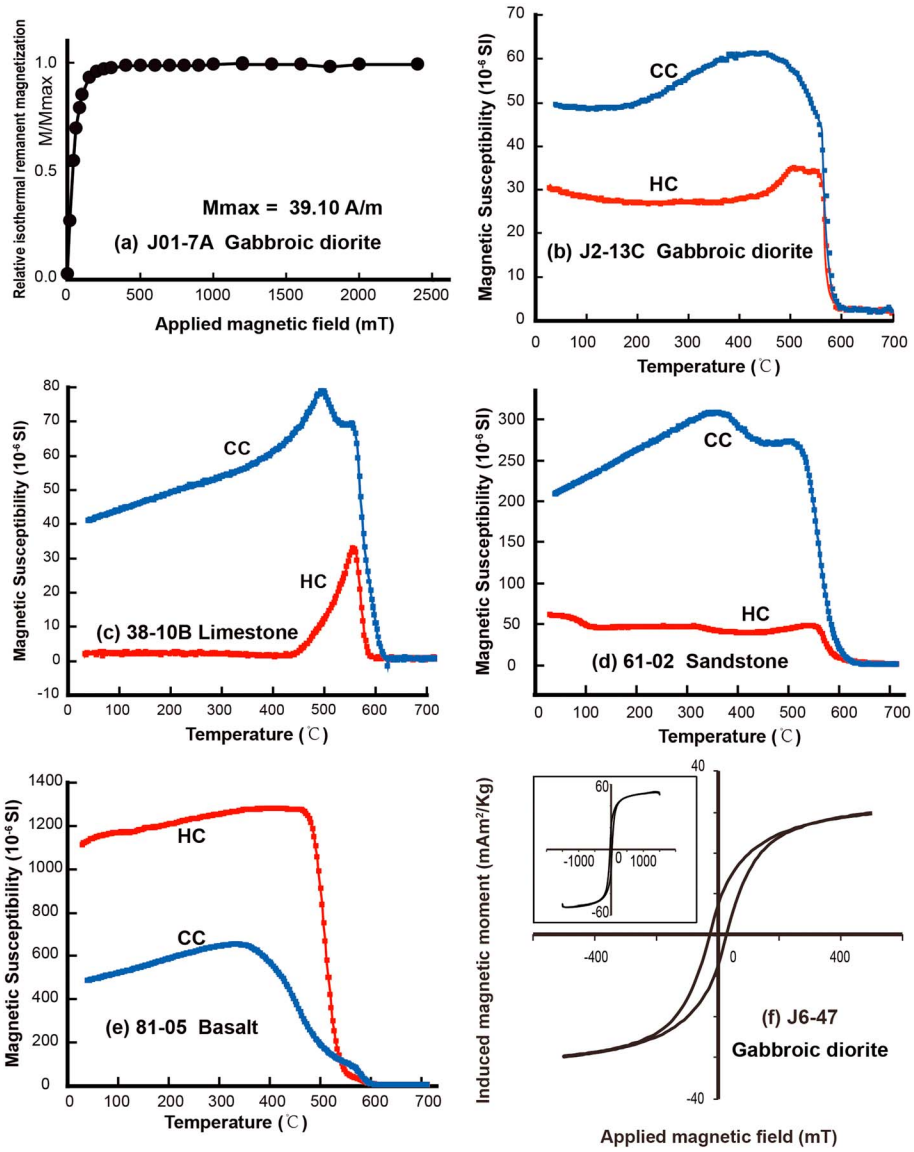

Figure 5. Results of different magnetic mineralogical studies indicating that magnetite and minor hematite are the principal magnetic carriers of studied rocks: (a) isothermal remanent magnetization acquirement curves, (b–e) thermomagnetic (Curie point) experiments, and (f) magnetic hysteretic curve.

analysis-calculated sample directions with Fisher spherical statistics (Fisher, 1953). The paleomagnetic data were analyzed with the software PMGSC (version 4.2 by R. Enkin, unpublished) and software packages offered by Cogné (2003).

3.3. Zircon U–Pb Geochronology

Zircons were extracted from crushed rock powders using techniques of heavy liquid and magnetic separation. The single zircon grains were handpicked under a binocular microscope and submerged into epoxy resin to form mount disks with a diameter of 1.2 cm. CL imaging was conducted at the State Key Laboratory of Continental Dynamics, Northwest University (Xi'an) with a Quanta 400 FEG scanning electron microscope equipped with a Gatan mini-CL detector (Mono CL3+).

U–Pb isotopic analyses were carried out on an Agilent 7500s inductively coupled plasma mass spectrometry coupled with a New Wave 193-μmlaser ablation system installed at the SKLMDR (Nanjing University). Two analyses of an internal zircon standard GJ (608 ± 1.5 Ma; Jackson et al., 2004) and one analysis of an

external zircon standard MudTank (732 ± 5 Ma; Black & Gulson, 1978) were made before and after each 10 analyses of unknown samples in order to trace instrument stability and to control analytical uncertainty.

Common Pb correction was carried out using the Microsoft Excel® embedded program ComPbCorr#3 15G (Andersen, 2002). The program ISOPLOT 3.1 add-in Microsoft Excel® was used for age calculation and Concordia plots. Uncertainties are quoted at 1σ for individual analyses and 2σ for weighted mean age calculation.

4. Results

4.1. Magnetic Mineralogical Investigations

The IRM acquisition curves of samples from mafic dikes show a rapid increase from 0 to 200 mT applied field, and the full saturation is reached at about 300 mT (Figure 5a), indicating the existence of low-coercivity magnetic minerals in the rocks. Thermal magnetic properties of all the measured samples are characterized by irreversible curves of magnetic susceptibility during heating and cooling, suggesting that magnetic mineral transformations occurred during the experiment (Figures 5b–5e). Figure 5b presents the characteristics of the thermal experiments for the dike samples. The progressive decrease in magnetic susceptibility from room temperature to about 400°C may suggest the presence of paramagnetic minerals. Rather significant increase in magnetic susceptibility between 450°C and 570°C probably resulted from mineral transformation from sulfide into magnetite. The rapid decrease of magnetic susceptibility from 570°C to 590°C indicates the existence of magnetite (Dunlop et al., 1997). No obvious change of magnetic susceptibility occurs after 590°C during the heating. However, a large and rapid increase in magnetic susceptibility is observed during cooling from 590°C to 400°C, which may be the result of the newly formed magnetite. Magnetic susceptibility shows a slightly decrease during the subsequent cooling, indicating possibly a phase change associated with iron sulfides (Roberts et al., 2011). The above characteristics suggest that magnetite is the main magnetic remanence carrier in the mafic dikes. Magnetic hysteresis loops corroborate this observation (Figure 5f).

Concerning the sedimentary rocks from the Early Permian sequences, a relatively small quantity of magnetite could be probably identified in limestone by a drop of magnetic susceptibility at about 580°C (Figure 5c), while the phenomenon of the newly formed magnetite was clearly observed from 430°C to 580°C (Figure 5c). By contrast, magnetite in sandstone is obviously shown in Figure 5d with a significant drop at 580°C. In addition, a weak and progressive decrease of the magnetic susceptibility after 580°C can also be recognized and indicates the existence of minor amounts of hematite.

As for the basalts, thermomagnetic curves prove that magnetite in variable sizes is the principal magnetic remanence carrier (Figure 5e). In addition, careful analysis of demagnetization curves (e.g., Figure 6h) reveals that variably important magnetic remanence remains after heating at 580°C, indicating the existence of hematite in the basalts.

4.2. Paleomagnetic Results

For the gabbroic diorite specimens from the mafic dikes, the range of the intensities of the natural remanent magnetization (NRM) is quite large, varying from 1.34×10^{-2} to 2.93 A/m. Most of the demagnetized specimens show a straightforward two component pattern with a low-temperature component (LTC) removed by ~200°C and a high-temperature component (HTC) isolated from 450°C to 590°C (Figure 6a). The results of AF demagnetization usually exhibit a simple single component pattern (Figure 6b). However, there are also some complex demagnetization curves (Figure 6c). The LTC directions are dispersed, indicating that they may be originated from viscous remanence. The HTC directions show exclusively reversed magnetic polarity and coherent magnetic directions; therefore, they can be considered as the characteristic remanent magnetizations (ChRMs). A few of them (about 8%) yielded erratic directions by thermal demagnetization due to possibly unstable magnetization or magnetic mineral transformation (Figure 6d); therefore, they are excluded from further statistical analysis.

Concerning the volcanic and sedimentary rocks in the Jinghe area, the NRM intensities of the basalts range from 3.63×10^{-3} to 6.15×10^{-2} A/m, and those of limestone specimens vary from 1.40×10^{-5} to 3.17×10^{-3} A/m. About one third of specimens yielded erratic directions and are excluded from further directional analysis. In the basaltic specimens, low coercivity components are generally removed by ~10 mT and are consistent with the present Earth field; therefore, they are interpreted as the present-day overprints

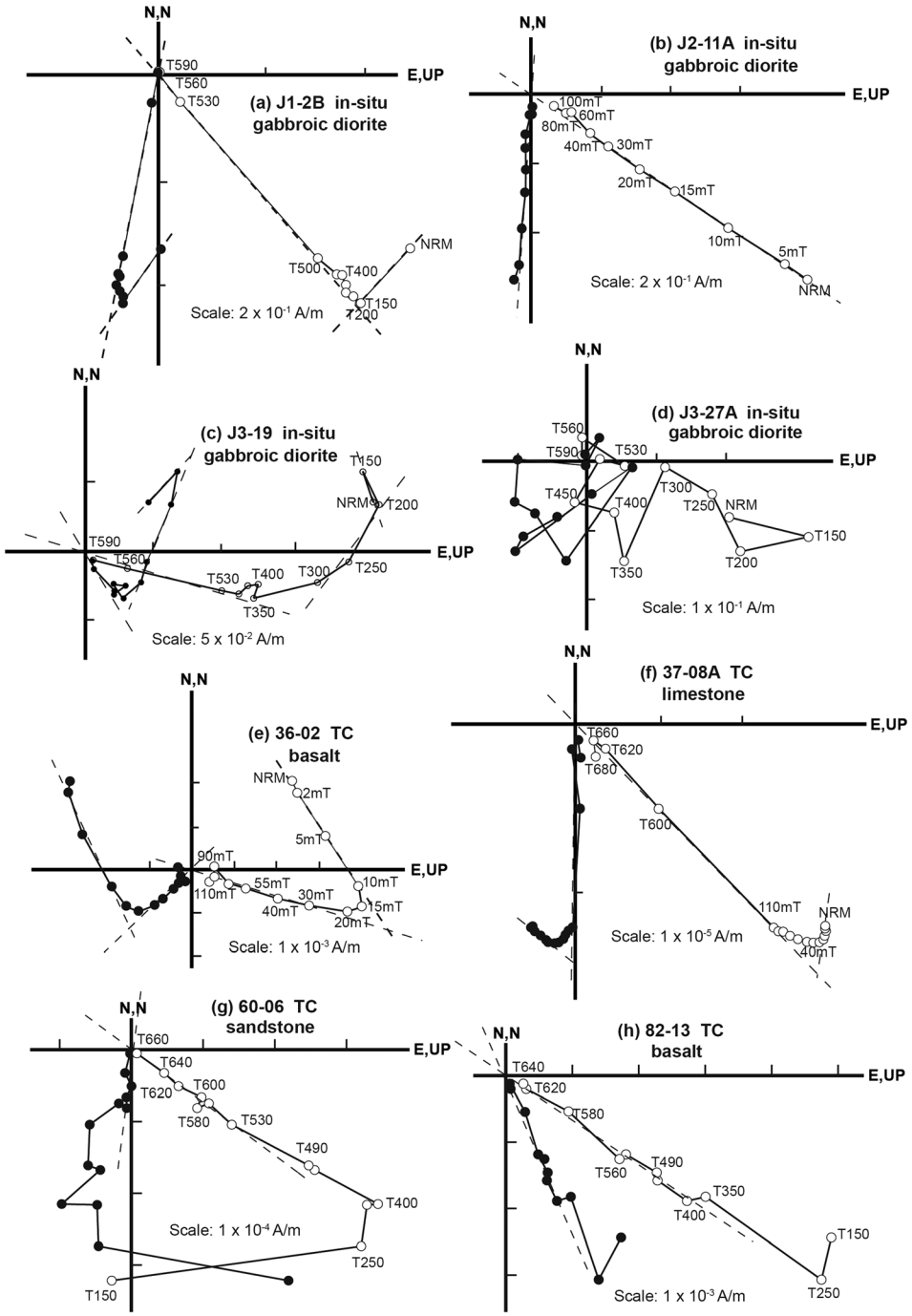

Figure 6. Plots of progressive demagnetization for representative samples of (a–d) Neoproterozoic mafic dikes), (e and f) Early Permian volcanic and sedimentary rocks from the Jinghe area, and (g and h) Nileke area. In situ and tilting-corrected stand for geographic coordinates and stratigraphic coordinates, respectively. The solid (open) circles show projections in the horizontal (vertical) plane.

(Figure 6e). High coercivity components are generally isolated from 30 to 70–100 mT (Figure 6e), representing the ChRMs of specimens. As the AF demagnetization cannot totally clean the remanence of the specimens from limestone, a supplementary thermal demagnetization was conducted, and ChRMs are successfully isolated at 660°C (Figure 6f).

For the samples from the Nileke area, the NRM intensities of basalts and sandstones range from 6.26×10^{-4} to 1.49×10^{-2} A/m and 1.03×10^{-4} to 1.07×10^{-3} A/m, respectively. Three specimens show erratic directions and are excluded from further analysis. From the remaining specimens, consistent HTCs are isolated from ~400°C to 560°C, and LTC directions of these specimens are quite dispersed (Figures 6g and 6h).

Mean directions of each site are calculated using Fisher spherical statistics, and the results are shown in Table 1.

4.3. Geochronological Results

The analytical data for zircon U–Pb age of the andesitic tuff sample 10W03A are shown in Table 2 and plotted in U-Pb Concordia diagram (Figure 7b). Thirteen concordant analyses yielded a mean age of 269.4 ± 2.4 Ma (MSWD = 1.3; Figure 7b). The dated zircons are 100–150 μm in size and have subhedral to euhedral shapes, and their CL images generally show clear concentric oscillatory zoning that is indicative of an origin from intermediate-acidic magma (Figure 7a; nos. 6, 17, 18, 19, 24, and 30). Ten additional euhedral to subhedral zircon grains (nos. 1, 3, 5, 7, 8, 9, 11, 12, 13, and 22) have sizes of 50–100 μm and are bright with unclear concentric oscillatory zoning (Figure 7a; nos. 3, 9, 12, and 22), and they yielded discordant ages (Table 2). The remaining seven zircon grains also yielded concordant ages, but they should have derived from different sources. Three zircons yielded relatively young ages (Figure 7a; Table 2; 258 Ma for zircon no. 15 and 215–230 Ma for nos. 25 and 29), and such young magmatic events are unknown in the study area; therefore, these three zircons were likely intermixed into the dated samples from external materials due to contamination. The zircon grain no. 4 yielded an extremely old age of ~2,200 Ma with a bright and blurry CL image which is totally different from the others (Figure 7a and Table 2). Relatively old ages (335–355 Ma) were obtained from three subhedral to euhedral zircons (nos. 26–28) with sizes of 100–150 μm and dark CL images (Figure 7a and Table 2). These old zircons should be xenocrysts derived from the magma source area or the underlying basement during the magmatism.

5. Discussion

Magnetic mineralogical experiments revealed both magnetite and hematite as the principal magnetic carriers in the Neoproterozoic mafic dikes and Early Permian volcanic and sedimentary rocks. Two component magnetizations have been successfully distinguished through progressive thermal and/or AF demagnetizations. The low-temperature and low-coercivity components show viscous and unstable magnetic remanences or a present-day overprint, whereas the high-temperature and high-coercivity components decay toward the origin and are considered as the ChRMs. All ChRMs exclusively show a reversed magnetic polarity. They are generally consistent within site and among sites as well (Table 1). Before analyzing the tectonic implications of these new paleomagnetic data, their reliability and magnetic remanence age will be discussed considering that the sampling areas experienced multiphase tectonic and magmatic events.

5.1. Reliability of the Magnetic Remanence Directions

Concerning the Early Permian (P_1) volcanic and sedimentary sequences, they show exclusive reversed magnetic polarity, which is coherent with the global magnetic polarity scale (Hounslow et al., 2004); field investigations did not reveal intensive deformation (only tilting), and no younger magmatism occurred in the study areas after the Early Permian. Therefore, the magnetic remanence directions of the P_1 volcanic and sedimentary rocks can be considered as the characteristic remanence.

The magnetic remanent directions of the Neoproterozoic mafic dikes are considered to be reliable, and these dikes were unaffected by deformation (probably only tilting) after their emplacement, or at least after the Early Permian, based on the following arguments: (1) Representative thin sections show that all minerals in the mafic dikes are subhedral to euhedral, implying the original magmatic fabrics, and no shape preferred orientation nor dynamic recrystallization could be observed (Figure 3h); (2) the subvertical geometry is a characteristic feature for the widespread Neoproterozoic mafic dikes in this region. Numerous dikes of similar ages are found in the NW and NE of Tarim, and these dikes did not experience a postemplacement folding (e.g., Chen, Xu, et al., 2004; Zhan et al., 2007); (3) the orogeny of the Tianshan Belt terminated in latest Carboniferous to earliest Permian (Han et al., 2011; Wang et al., 2008; Wang, Shu, et al., 2011), and no significant tectonic event occurred after the Early Permian in the studied area. Post-Permian crustal shortening in

Tectonics

10.1029/2017TC004642

Table 2
Zircon Laser Ablation-Inductively Coupled Plasma Mass Spectrometry U–Pb Analytical Results of the Early Permian Andesitic Tuff (Sample 10W03A)

	Corrected isotopic ratios						Corrected apparent ages (ma)							
Analysis no.	$^{207}Pb/^{206}Pb$	1σ	$^{207}Pb/^{235}U$	1σ	$^{206}Pb/^{238}U$	1σ	$^{207}Pb/^{206}Pb$	1σ	$^{207}Pb/^{235}U$	1σ	$^{206}Pb/^{238}U$	1σ	Error correlation	Comments
10w03a-01	0.05517	0.00158	0.31295	0.00797	0.04114	0.00053	419	65	276	6	260	3	0.43	Discordant
10w03a-02	0.0519	0.00149	0.30449	0.00782	0.04255	0.00054	281	67	270	6	269	3	0.46	
10w03a-03	0.06155	0.00788	0.3379	0.0426	0.03981	0.00088	659	287	296	32	252	5	0.63	Discordant
10w03a-04	0.14109	0.00186	7.97861	0.11723	0.41019	0.00535	2241	23	2229	13	2216	24	0.55	Inheritance
10w03a-05	0.05836	0.00093	0.34882	0.00596	0.04336	0.00057	543	36	304	4	274	4	0.47	Discordant
10w03a-06	0.05198	0.00134	0.30479	0.00683	0.04253	0.00054	284	60	270	5	268	3	0.43	
10w03a-07	0.06801	0.0051	0.35633	0.02588	0.038	0.0007	869	160	309	19	240	4	0.39	Discordant
10w03a-08	0.05726	0.00166	0.33403	0.00957	0.04231	0.00064	502	65	293	7	267	4	0.24	Discordant
10w03a-09	0.06261	0.0078	0.35049	0.04287	0.0406	0.00096	695	279	305	32	257	6	0.47	Discordant
10w03a-10	0.05466	0.00081	0.3316	0.00537	0.04401	0.00057	398	34	291	4	278	4	0.5	
10w03a-11	0.05582	0.00084	0.34448	0.00574	0.04477	0.0006	445	34	301	4	282	4	0.52	Discordant
10w03a-12	0.07676	0.00136	0.28651	0.00536	0.02707	0.00038	1115	36	256	4	172	2	0.44	Discordant
10w03a-13	0.06249	0.00249	0.35962	0.01395	0.04174	0.00074	691	87	312	10	264	5	0.17	Common Pb
10w03a-14	0.05306	0.00074	0.31377	0.00494	0.04289	0.00057	331	32	277	4	271	4	0.55	
10w03a-15	0.05264	0.00169	0.29645	0.00865	0.04085	0.00054	313	75	264	7	258	3	0.47	Contamination
10w03a-16	0.05418	0.00166	0.32266	0.00892	0.0432	0.00058	378	71	284	7	273	4	0.48	
10w03a-17	0.05468	0.00083	0.31966	0.00535	0.04241	0.00057	399	35	282	4	268	4	0.51	
10w03a-18	0.05267	0.00081	0.30599	0.00517	0.04214	0.00056	315	36	271	4	266	3	0.5	
10w03a-19	0.05197	0.00082	0.30955	0.00535	0.04321	0.00058	284	37	274	4	273	4	0.5	
10w03a-20	0.05327	0.00099	0.3219	0.00631	0.04383	0.0006	340	43	283	5	277	4	0.42	
10w03a-21	0.05379	0.00078	0.31125	0.00501	0.04197	0.00055	362	33	275	4	265	3	0.52	
10w03a-22	0.05714	0.00117	0.33198	0.00706	0.04214	0.00059	497	46	291	5	266	4	0.38	Discordant
10w03a-23	0.05075	0.0023	0.29726	0.01267	0.04248	0.00065	230	107	264	10	268	4	0.42	
10w03a-24	0.05481	0.00074	0.31994	0.0049	0.04234	0.00055	404	31	282	4	267	3	0.56	
10w03a-25	0.05255	0.00182	0.26157	0.00829	0.0361	0.0005	309	81	236	7	229	3	0.37	Contamination
10w03a-26	0.05316	0.00254	0.39341	0.01782	0.05367	0.00083	336	111	337	13	337	5	0.45	Inheritance
10w03a-27	0.05483	0.00086	0.42619	0.00733	0.05637	0.00075	405	36	360	5	354	5	0.5	Inheritance
10w03a-28	0.05266	0.00077	0.38481	0.00626	0.053	0.0007	314	34	331	5	333	4	0.52	Inheritance
10w03a-29	0.04955	0.00214	0.23326	0.00951	0.03414	0.00049	174	101	213	8	216	3	0.33	Contamination
10w03a-30	0.05249	0.00179	0.30392	0.00935	0.042	0.00062	307	80	269	7	265	4	0.27	

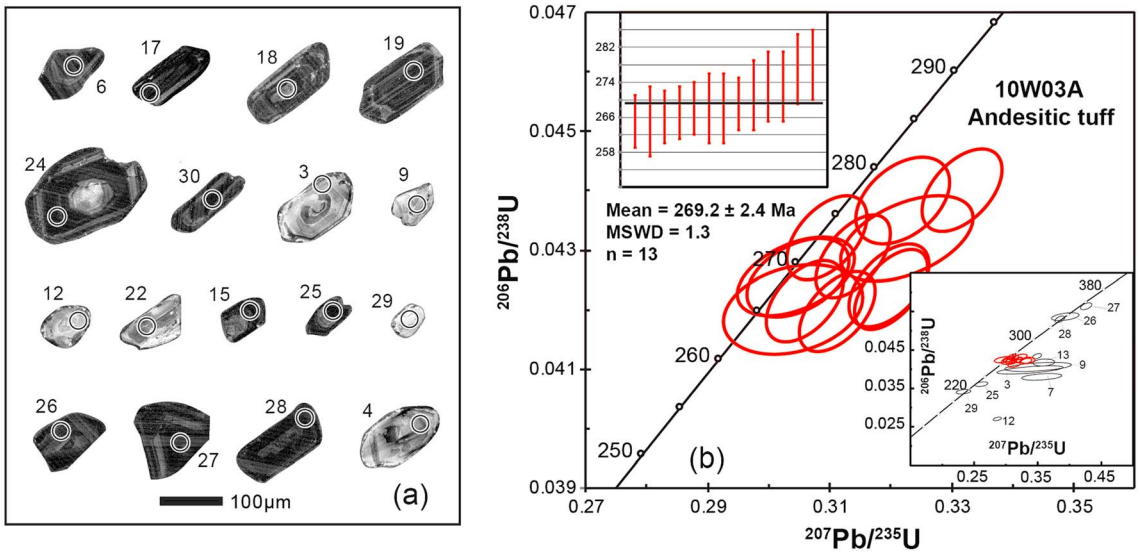

Figure 7. (a) Representative cathodoluminescence images and (b) Concordia diagram of dated zircon grains (by laser ablation-inductively coupled plasma mass spectrometry U–Pb method) from the andesitic tuff in the northern Yili Block. See Table 2 for the isotopic ratios and ages of individual analyses.

the study area was linked to the Cenozoic India-Asia collision and is characterized by thin-skinned structures (broad and gentle folds; e.g., Avouac & Tapponnier, 1993).

5.2. Age of Magnetic Remanence and Paleomagnetic Pole Calculation

Although the andesitic tuff is dated at ~270 Ma, which can be used to constrain the overall formation age of the volcanic and sedimentary sequences of the Jinghe area, and the regional stratigraphic relationship has been characterized for the volcanic and sedimentary sequences in the Jinghe and Nileke areas (XBGMR, 1993), it is necessary to ensure if the magnetic remanence is primary in order to determine its age. Thus, we carried out a careful analysis on the demagnetization curves, and then performed fold tests (Figure 8).

By careful analysis on the demagnetization curves, substantial amount of hematite is suggested to exist in the Early Permian sedimentary and basaltic volcanic rocks. For the sedimentary rocks, two components can be separated above and below 580°C, and their difference is generally too small to be significant for a paleomagnetic study (commonly less than 5° and up to 10° for the extreme case of sample 60–06; Figure 6g). Two possibilities could explain such small difference: (i) experimental errors as the magnetic remanence intensity decreased significantly at high temperature, which would imply that these two components can be considered parallel, and (ii) the component carried by hematite is a chemical remanence acquired shortly after deposition, representing the postdepositional remanent magnetization (Butler, 1992; Tauxe et al., 2010), which is commonly found in many sedimentary environments and is often considered as an accurate recorder of the geomagnetic field at or very close to the time of deposition (Butler, 1992). In the case of our basaltic volcanic rocks showing two indistinguishable remanence components isolated above and below 580°C, two possible processes for remanence acquisition can be proposed: (i) Hematite carries a chemical magnetic remanence obtained by oxidation soon after the lava emplacement and (ii) both magnetite and hematite carry a simple remagnetization. The latter is inconsistent with the regional geology; that is, no regional magmatism or high-temperature metamorphism was documented after Early Permian in the study area. In addition, as aforementioned, sedimentary samples in the vicinity or the same sampling sites demonstrate no remagnetization characteristics.

Stepwise unfolding of the Nileke strata shows that the precision parameter (k) reaches maximum (k_{max} = 18.54) at 116% unfolding with a positive response to the Enkin's fold test (Enkin, 2003; Figures 8a and 8b). The k values are 17.54 after unfolding (k_s) and 5.72 before unfolding (k_g). The variance ratio $f = k_s/k_g$ = 3.07 is between 2.69 at the 95% confidence limit and 4.16 at the 99% confidence limit for N = 7 (the number of directions of magnetization) (McElhinny, 1964). Thus, a positive fold test at 95% confidence interval is also supported by McElhinny (1964). On the contrary, the k value of the Jinghe strata is highest (k_{max} = 75.27) at 43.3%

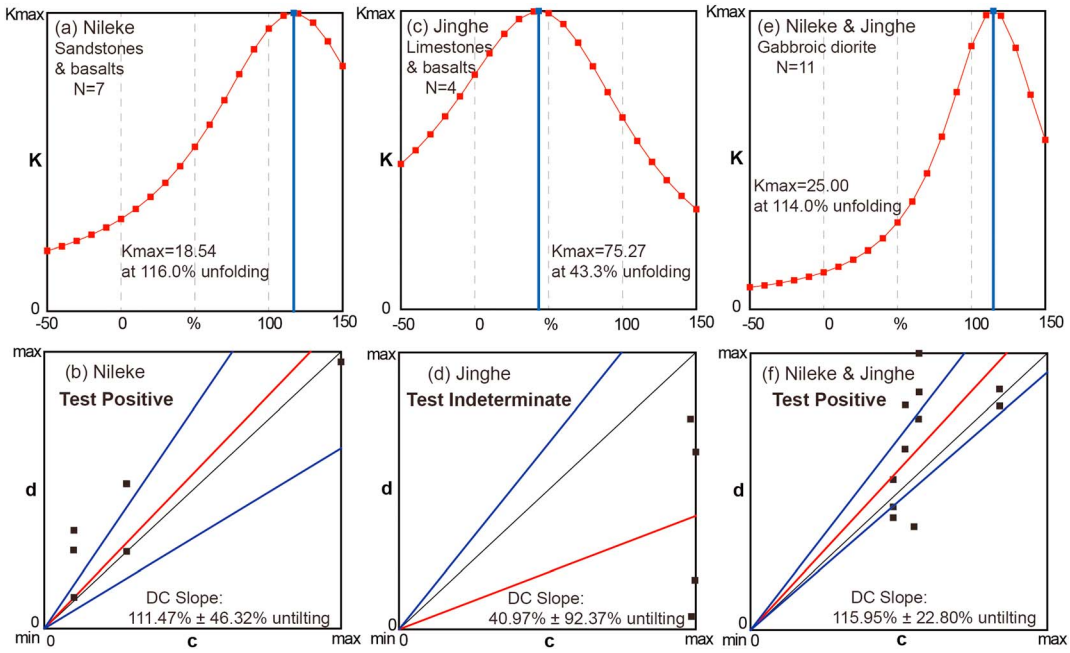

Figure 8. Progressive unfolding (PMGSC 4.2 by R. Enkin) and direction-correction test (Enkin, 2003) of the characteristic remanent magnetizations for the Early Permian volcanic and sedimentary samples collected from (a and b) the Nileke area, (c and d) the Jinghe area, and (e and f) both Jinghe and Nileke areas.

unfolding (Figures 8c and 8d), indicating a probable "synfolding" process; however, different variance ratios are calculated at $f_1 = k_s/k_g = 1.22$, $f_2 = k_{max}/k_s = 1.55$, and $f_3 = k_{max}/k_g = 1.27$; all these variance ratios are obviously lower than the 95% and 99% confidence limits (4.28 and 8.47, respectively) for $N = 4$ (McElhinny, 1964). Thus, an inconclusive fold test is suggested based on both Enkin (2003) and McElhinny (1964). When the samples from both Nileke and Jinghe areas are analyzed together, the optimal k value ($k_{max} = 25.00$) is at 114% unfolding with a positive response to the fold test (Enkin, 2003; Figures 8e and 8f) and at 99% confidence interval according to McElhinny (1964), corresponding an $f = k_s/k_g = 22.12/2.99 = 7.40$, higher than the 95% and 99% confidence limits for $N = 11$ (2.12 and 2.94, respectively). Statistically, the grouping at 114% is indistinguishable with that at 100%, suggesting a prefolding remanence.

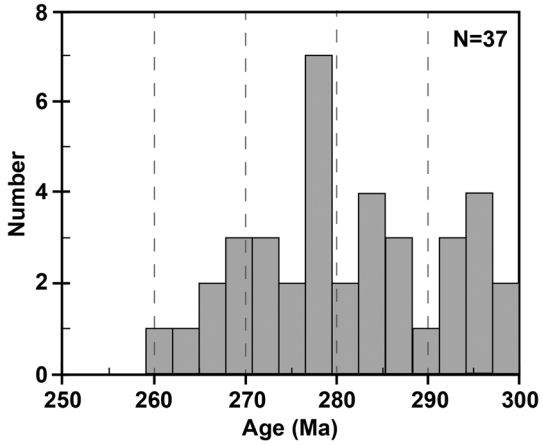

Figure 9. The age distribution diagram of the Permian magmatism in the Yili Block (age data from Chen et al., 1994, 2004, 2007; Chen, Xu, et al., 2004; Duan et al., 2014; Gao et al., 2006, 2009; Gou et al., 2015; Li et al., 2012, 2013, 2015; Liu et al., 2005; Long et al., 2011; Tang et al., 2010; Wang et al., 2004, 2009; Wang, Chen, et al., 2007; Wang, Shu, et al., 2007; Xu et al., 2006, 2013; Yang et al., 2012; Zhang et al., 2008; Zhang, Tian, et al., 2012; Zhang, Zhang, et al., 2012; Zhao, Bai, et al., 2003).

The fold test on the Jinghe section presents a rather delicate situation, and an original environment on a slope for the volcanic and sedimentary rocks could be one of possibilities, but we need additional study to test. The inconclusive fold test is also probably due to the weak bedding variation and small number of sites. In addition, considering that (1) the study area did not experience important deformation nor thermal reactivation events after Early Permian; (2) their remanence magnetization directions are consistent with those of coeval strata from the Nileke area; and (3) there is a good consistency between the pole calculated by tilt-corrected directions and other previous paleomagentic poles of the Yili Block (Wang, Chen, et al., 2007), the magnetic remanence of the Jinghe section could be considered as primary. Consequently, the ChRMs of volcanic and sedimentary sequences from both the Nileke and Jinghe areas are more likely primary.

For the Neoproterozoic mafic dikes, we prefer to consider that their magnetic remanence resulted from the Early Permian remagnetization

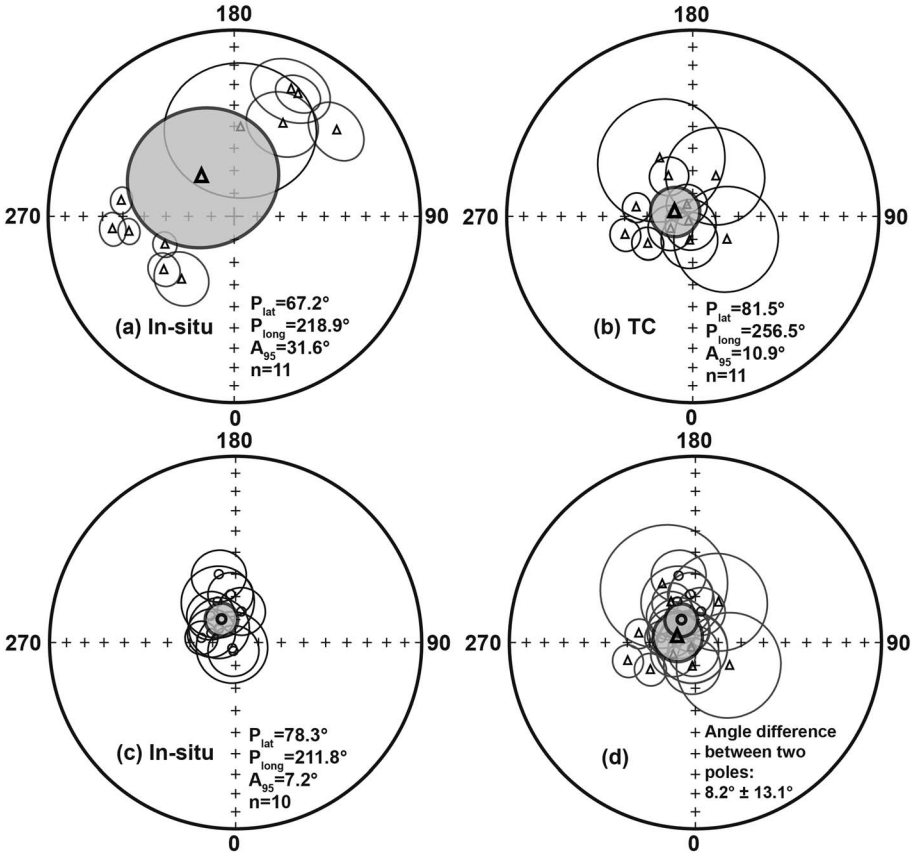

Figure 10. Equal-area projections of visual geomagnetic poles (VGPs) from the Early Permian volcanic and sedimentary rocks in (a) geographic and (b) stratigraphic coordinates and from the Neoproterozoic mafic dikes in the (c) geographic coordinate; (d) comparison of the tilting-corrected pole calculated from the Early Permian volcanic and sedimentary rocks with the in situ pole of the Neoproterozoic mafic dikes. The triangle (circle) symbols show poles from volcanic and sedimentary rocks (mafic dikes), and the shadowed plots stand for the mean poles. Note: No tilt corrections are made on the VGPs from the Neoproterozoic mafic dikes due to the uncertainty of their magnetic remanence age.

on the basis of the following arguments: (1) A good coherence is observed between the tilt-corrected directions of the P_1 strata and the in situ directions of the mafic dikes (Table 1); (2) in the Jinghe area, about 5–10 km apart from the dikes, unconformable contact can be easily observed between the P_1 sequence of the Wulang Group and the Neoproterozoic Kairtas Group in which the mafic dikes intruded (XBGMR, 1988a; Figure 4a); and (3) intense magmatic activities occurred in the study area during the Carboniferous and Permian. Figure 9 shows the age compilations of the Permian magmatic activities in the Yili Block, and the peak of the magmatism is at ~280 Ma. Such massive magmatism and related fluid activities may have easily affected the Neoproterozoic mafic dikes, resulting in their remagnetization.

However, considering the possibly fast cooling of the studied mafic dikes (Silva et al., 2006), the polarity ambiguity due to the insufficiency of Precambrian paleomagnetic results (Driscoll & Evans, 2016), and lack of coeval paleomagnetic data from the study block, it is impossible to definitely rule out a primary-ChRMs in the mafic dikes. Thus, further studies are needed to better constrain the age of the magnetic remanence of these Neoproterozoic dikes.

Consequently, we calculated two paleomagnetic poles: one for the Early Permian strata (81.5°N, 256.5°E, N = 11 and A_{95} = 10.9°; Table 1 and Figures 10a and 10b) and one for the Neoproterozoic mafic dikes (78.3°N, 211.8°E, N = 10 and A_{95} = 7.2°; Table 1 and Figure 10c). The poles are statistically indistinguishable with an angular difference of 8.2° ± 13.1° (Figure 10d). Furthermore, since the Early Permian remagnetization of the Neoproterozoic dikes is not yet proved, we will apply only the paleomagnetic pole calculated from the

Table 3
Compilations of Late Carboniferous to Late Permian Paleomagnetic Poles From the Yili, Tarim, and South Junggar Blocks

Blocks	Areas	Ages	*N*	S-Lat (°N)	S-Long (°E)	P-Lat (°N)	P-Long (°E)	A_{95} (°)	References
Yili	Mean[a]	C_2	15			68.6	290.6	6.1	Wang, Chen et al. (2007)
	Mean[b]	P_1	11			81.5	256.5	10.9	This study
	Gongliu	P_2	5	43.4	82.5	79.7	172.0	11.3	Wang, Chen et al. (2007)
Tarim	Mean[c]	C_2				51.5	169.1	7.7	Wang, Chen et al. (2007)
	Mean[d]	P_1				59.7	175.1	7.1	Zhao et al. (2014)
	Mean[e]	P_2				66.8	184.1	4.9	Wang, Chen et al. (2007)
South	Urumqi	C_2	15	43.8	87.8	71.9	4.7	13.3	Li et al. (1991)
Junggar	Urumqi	P_1	4	43.8	87.8	79.5	36.6	6.8	Choulet et al. (2011)
	Urumqi	P_2	4	43.8	87.8	75.0	13.3	22.1	Sharps et al. (1992)
	Urumqi[f]	P_2	78 s	43.8	87.8	77.7	0.5	5.5	Sharps et al. (1992)
	Urumqi	P_2	6	43.8	87.8	60.4	4.7	5.4	Choulet et al. (2011)
	Tianzhi[g]	P_2	7	44.0	88.1	76.0	193.0	16.2	Nie et al. (1993)
	Tianchi[g]	P_2	6	43.9	88.1	80.0	191.6	12.4	Choulet et al. (2013)
	Mean	P_2	3			71.1	6.1	14.5	This study

Notes. Abbreviations: *S-Lat/S-Long*, latitude/longitude of sampling sites. *P-Lat/P-Long*, latitude/longitude of paleomagnetic poles. A_{95} is the radius with which mean directions lies within 95% confidence. *N* is the number of sites.
[a]Mean of poles obtained from the Zhaosu and Xinyuan areas, southern Yili Block (Wang, Chen, et al., 2007). [b]Mean of poles obtained from the Jinghe and Nileke areas, northern and central Yili Block (this study). [c]Mean of poles from Sharps et al. (1992), Voo (1993), Nie et al. (1993), Gilder et al. (1996), and Hankard et al. (2005). [d]Mean of poles from Bai et al. (1985), Sharps et al. (1989), Gilder et al. (1996), and Fang et al. (1998). [e]Mean of poles from Li et al. (1989), Li et al. (1991), Meng (1991), and Gilder et al. (1996). [f]Pole calculated from 52 out of 78 samples analyzed with great circle method. [g]Poles not used for calculating the P_2 mean pole of the south Junggar. For more details, see discussion section 5.3.

Early Permian volcanic and sedimentary rocks in the following tectonic interpretations. This is the first Early Permian paleomagnetic pole for the Yili Block.

5.3. Comparisons of Paleomagnetic Poles Between the Yili Block and the Adjacent Blocks

Until about 10 years ago, no paleomagnetic data were documented from the Yili Block. Some results were obtained from Permo-Carboniferous rocks in the western Kyrgyz Tianshan (Bazhenov et al., 1993, 1999, 2003), and most of the samples were collected from the orogenic belt where local rotations took place along major faults within the tectonic belt; therefore, they cannot represent the Yili Block (Bazhenov et al., 1999; Wang, Chen, et al., 2007). Conducting the first paleomagnetic study on the sedimentary and volcanic rocks from the Yili Block, Wang, Chen, et al. (2007) provided Late Carboniferous and Late Permian paleomagnetic poles for the Yili Block. In this study, we obtain an Early Permian pole that may provide more data for unraveling the late Paleozoic kinematic evolution of this block with respect to the neighboring ones (Table 3).

Table 3 presents a synthesis of paleomagnetic poles of Late Carboniferous (C_2), Early Permian (P_1), and Late Permian (P_2) from the Tarim, Yili, and South Junggar blocks. Among the 5 Late Permian poles of the South Junggar Block, the former three are consistent (Table 3; Choulet et al., 2011; Sharps et al., 1992). The fourth one comes from Nie et al. (1993) and is significantly different from the former three. Choulet et al. (2013) conducted a paleomagnetic study basically in the same area as Nie et al. (1993) and acquired another Late Permian paleomagnetic pole which is indistinguishable from that of Nie et al. (1993) with an angular difference of 4.0 ± 20.4°. Based on regional geology and stratigraphic observations, Choulet et al. (2013) considered that the studied strata could have underwent local rotation during syn-tectonic sedimentation. Accordingly, the latter two poles have been removed from the mean pole calculation, and the mean P_2 pole for the South Junggar Block is recalculated at 71.1°N, 6.1°E, A_{95} = 14.5° (Table 3). It is also worth noting that the P_1 pole for the South Junggar may be questionable as it was acquired from only four sites.

Figure 11 shows the mean paleomagnetic poles of the Yili, Tarim, and South Junggar blocks for the C_2, P_1, and P_2 periods. The distribution of these poles seems quite dispersed with significant angular differences until the Late Permian. For the Late Carboniferous, the pole of the Yili Block is 52.3° ± 7.2° and 23.0° ± 10.7° away from those of the Tarim and South Junggar blocks. The angular differences between the Yili poles and the poles of the Tarim and South Junggar blocks progressively decrease to 29.7° ± 9.5° and 17.2° ± 9.4° for the Early Permian, then to 12.5° ± 9.0° and 28.2° ± 13.5° for the Late Permian, respectively (Table 4).

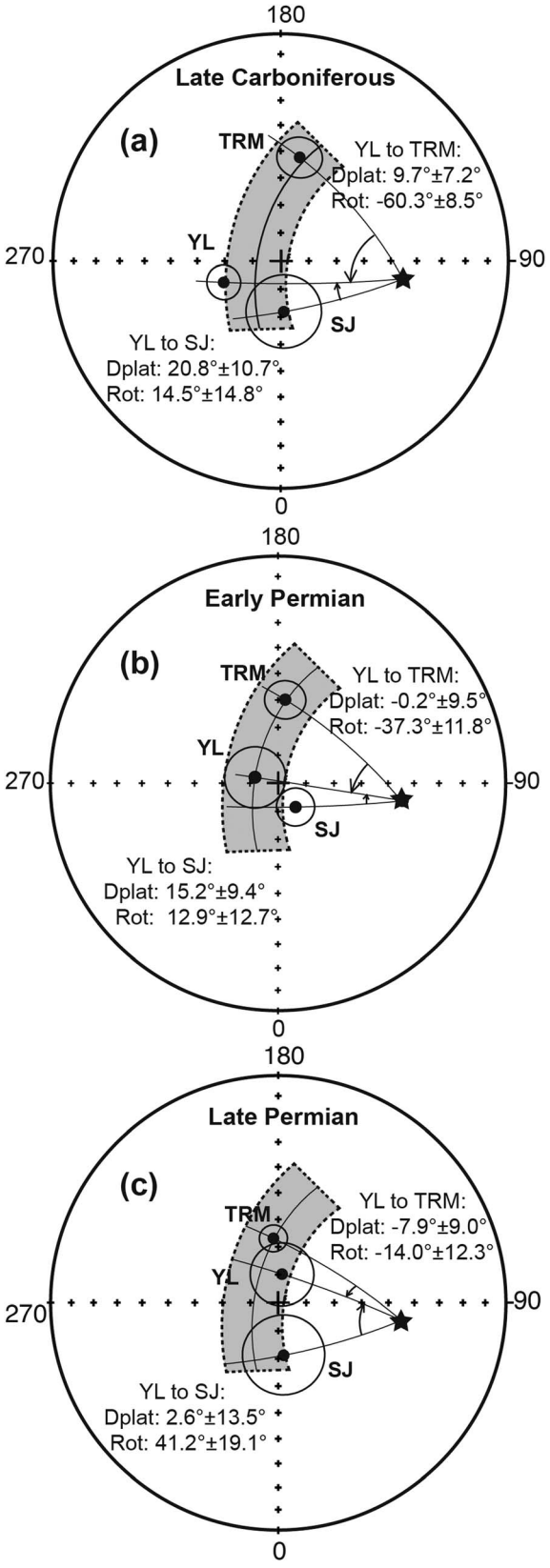

However, the above-mentioned paleomagnetic poles are mainly distributed along small circles centered at the sampling sites. In other words, these polar angular differences may essentially correspond to the relative rotations and the movements along block boundaries, while the crustal shortening among these blocks is relatively weak or negligible. The relative rotations of the Yili Block with respect to the Tarim and South Junggar blocks are calculated as −60.3° ± 8.5° and 14.5° ± 14.8°, −37.3° ± 11.8° and 12.9° ± 12.7°, and −14.0° ± 12.3° and 41.2° ± 19.1° since C_2, P_1, and P_2, respectively (Figure 11). The latitudinal movements of the Yili Block with respect to the Tarim and South Junggar blocks are estimated as 9.7° ± 7.2° and 20.8° ± 10.7°, −0.2° ± 9.5° and 15.2° ± 9.4°, and − 7.9° ± 9.0° and 2.6° ± 13.5° since C_2, P_1, and P_2, respectively (Table 4 and Figure 11).

5.4. New Quantitative Constraints on the Late Paleozoic Kinematic Evolution of the SW CAOB and its Tectonic Implications

Wang, Chen, et al. (2007) conducted the first quantitative estimation on the relative movements among the three major blocks in the SW CAOB (the Yili, Tarim, and Junggar blocks). Due to limited data from the Yili and Junggar blocks, they grouped the paleomagnetic poles for the Late Carboniferous and the Late Permian stages and concluded that these blocks shared similar latitudes but experienced differential rotations during a single C_2-P_2 period. With newly obtained Paleozoic and Mesozoic paleomagnetic poles from the south and west Junggar areas, Choulet et al. (2011) argued that the Junggar domain cannot be considered as a rigid block at least until the end of the Paleozoic, and only the South Junggar experienced a similar tectonic evolution with the Yili and Tarim blocks in the late Paleozoic. Our new P_1 paleomagnetic results for the Yili Block allow us to depict a more detailed kinematic history among these blocks.

According to our and the previous paleomagnetic results, the relative movements between these major blocks are indicated by changes of angular differences between their paleomagnetic poles with the time. For the Yili and Tarim blocks which are separated by the Nikolaiev Tectonic Line (NTL; e.g., Burtman, 1975) and the Nalati Fault (Gao et al., 2009; Wang et al., 2008, 2010), a significant rotation with a weak latitudinal movement occurred during C_2 to P_1, and an equally important rotation but no obvious latitudinal movement happened from P_1 to P_2 (Table 4 and Figure 11). The Yili Block shows a counter clockwise rotation of 23.0° ± 11.6° and a northward movement of 9.9° ± 9.5° with respect to the Tarim Block during the C_2-P_1 period. These results are quite consistent with the dextral kinematics along the NTL and Nalati Fault (e.g., Wang et al., 2008, 2010; Wang, Chen, et al., 2007; Yin & Nie, 1996). The timing of rotation is also in agreement with the available $^{40}Ar/^{39}Ar$ age obtained along the NTL and Nalati Fault (286.4 ± 2.4 Ma; Laurent-

Figure 11. Equal-area projections of paleomagnetic poles of the Yili (YL), Tarim (TRM), and South Junggar (SJ) blocks in (a) Late Carboniferous, (b) Early Permian, and (c) Late Permian. Dplat and Rot stand for convergence and relative rotation (with corresponding uncertainties), respectively. The positive (or negative) mean values stand for latitudinal shortening (or extension) or clockwise (counterclockwise) rotation, respectively. More details can be found in sections 5.3 and 5.4.

Table 4
Relative Movements of the Yili Block With Respect to the Surrounding Blocks During the Late Paleozoic

Period	Blocks	Angle difference (°)	Plat ± Δplat (°)	ROT ± ΔROT (°)
C_2	YL versus TRM	52.3 ± 7.2	9.7 ± 7.2	−60.3 ± 8.5
	YL versus SJ	23.0 ± 10.7	20.8 ± 10.7	14.5 ± 14.8
P_1	YL versus TRM	29.7 ± 9.5	−0.2 ± 9.5	−37.3 ± 11.8
	YL versus SJ	17.2 ± 9.4	15.2 ± 9.4	12.9 ± 12.7
P_2	YL versus TRM	12.5 ± 9.0	−7.9 ± 9.0	−14.0 ± 12.3
	YL versus SJ	28.2 ± 13.5	2.6 ± 13.5	41.2 ± 19.1

Notes. Abbreviations: YL, SJ, and TRM stand for the Yili Block, South Junggar Block, and Tarim Block, respectively. Plat ± Δplat and ROT ± ΔROT correspond to relative latitudinal displacement and rotation (and their errors) between blocks. Note that the relative movements between the blocks are computed using an average sampling site at: 44.2°N, 82.0°E.

Charvet et al., 2003; Yin & Nie, 1996). Wang, Chen, et al. (2007) and Choulet et al. (2011) suggested that the relative rotations were accommodated by large movements along the major ductile shear zones, and the Euler pole of this relative movement is located to the north of these blocks. Thus, the relative rotation between these two blocks could be accommodated by an eastward extrusion of the Yili Block with respect to the Tarim Block. Moreover, as the NTL and Nalati Fault strike NE-SW, the weak northward movement of the Yili Block with respect to the Tarim Block might occur as a simple "sliding" along the fault instead of a crustal shortening. Assuming that the NTL and Nalati Fault kept the same shape during C_2-P_1 as that described in Wang, Chen, et al. (2007) for C_2-P_2, the Euler pole documented by Wang, Chen, et al. (2007) can be adopted to estimate the movement along these faults. With a radius of about 1440 km and a rotation angle of 23.0° ± 11.6°, the lateral displacement during C_2-P_1 (300–270 Ma) is calculated at 580 ± 290 km, corresponding to a displacement rate of ~19.3 ± 9.7 mm/yr (Figures 12a and 12b). Since then, the relative

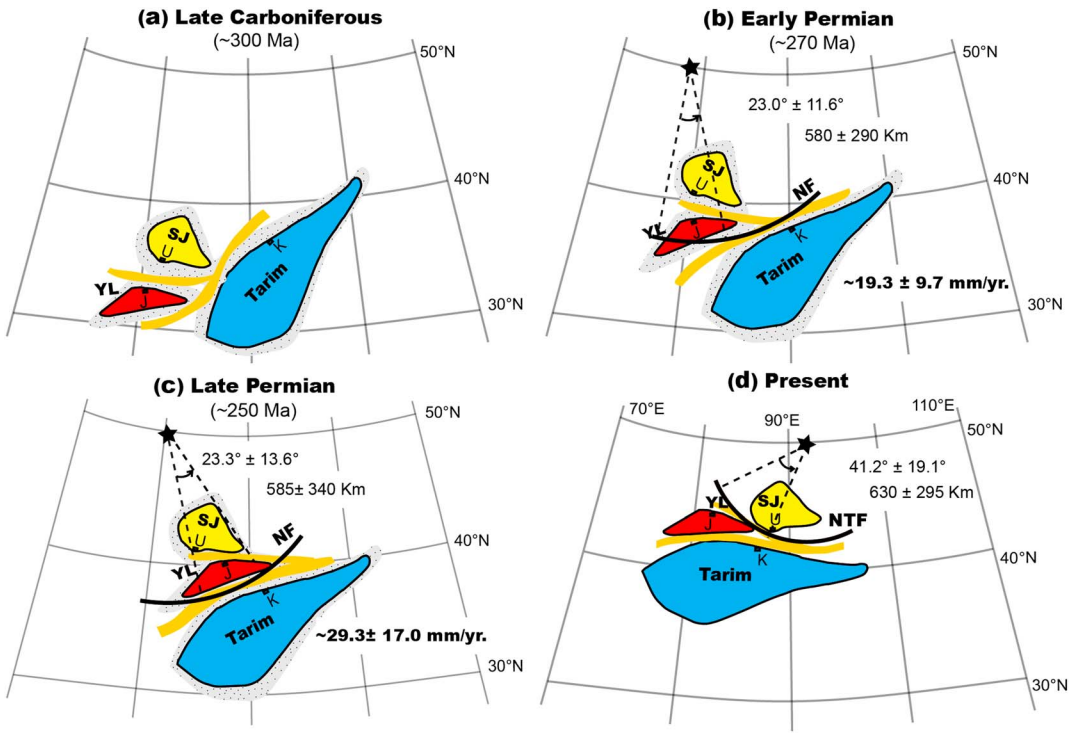

Figure 12. Tentative paleogeographic reconstruction maps of the Yili, Tarim, and South Junggar blocks for (a) Late Carboniferous, (b) Early Permian, (c) Late Permian, and (d) present with the relative movements. The shadowed zones around each block indicate the loss of continental margin during Cenozoic intracontinental deformation. J, K, and U stand for the positions of Jinghe, Korla, and Urumqi cities, respectively.

rotation between two blocks continued (−23.3° ± 13.6°) from P_1 to P_2 but the latitudinal movement became negligible (7.7° ± 10.5°). This is consistent with the dextral strike-slip faulting along the Nalati Fault that was still active at least up to 250 Ma as suggested by $^{40}Ar/^{39}Ar$ dating results (de Jong et al., 2009; Wang et al., 2010). Similarly, using an Euler pole radius of 1,440 km and a rotation angle of 23.3° ± 13.6°, the lateral displacement during P_1-P_2 (270–250 Ma) along this fault can be estimated at 585 ± 340 km. The corresponding displacement rate is calculated as ~29.3 ± 17.0 mm/yr (Figures 12b and 12c).

The Yili and South Junggar blocks are separated by the NTF (e.g., Zhou et al., 2001; Zhao, Liu, et al., 2003; Wang et al., 2006, 2009; Wang, Chen, et al., 2007) that extends eastward and merges into the Main Tianshan Shear Zone (Laurent-Charvet et al., 2002, 2003). Dextral sense of movement was observed along these faults (Laurent-Charvet et al., 2002, 2003; Wang et al., 2006, 2009; Wang, Chen, et al., 2007). $^{40}Ar/^{39}Ar$ dating constrained the deformation ages from 290 to 240 Ma (de Jong et al., 2009; Laurent-Charvet et al., 2002, 2003; Yin & Nie, 1996; Zhou et al., 2001). In the same way, we calculated the relative latitudinal movement and rotation between Yili and South Junggar during C_2 to P_1 period as 5.6° ± 11.4° and 1.6° ± 15.6° and during the P_1 to P_2 as 12.6° ± 13.2° and −28.3° ± 18.3°, respectively. The tectonic interpretation of these calculations must be cautiously made because the paleomagnetic data from South Junggar are still scarce and the quality of current poles needs to be reinforced. Keeping the large uncertainties in mind, no significant change of angular differences between the C_2 poles and P_1 poles of two blocks can be recognized (Figures 11a and 11b), indicating that no relative movement occurred between two blocks during C_2 to P_1, likely because both blocks moved with similar directions and magnitudes. By contrast, angular differences between the P_2 poles of two blocks are obviously distinct from the angular differences of their P_1 poles, and a significant counterclockwise rotation of −28.3° ± 18.3° of the Yili Block with respect to the South Junggar Block can be calculated (Figures 11b and 11c and 12b and 12c). Such remarkable relative rotation was probably resulted from obviously different motions both in directions and in magnitudes of two blocks during P_1 to P_2 period. Furthermore, our analysis reveals that the Yili Block experienced a large rotation of 41.2° ± 19.1° with respect to South Junggar along the NTF after the Late Permian. This large relative rotation corresponds to a lateral displacement of 630 ± 295 km on the basis of the Euler pole defined by Choulet et al. (2011) with a radius of 880 km (Figures 12c and 12d). This result confirms the paleomagnetic study by Choulet et al. (2011), showing that the dextral shearing continued after the Late Permian and is consistent with the dextral motion of the NTF whose timing is dated at the Early Triassic by $^{40}Ar/^{39}Ar$ method (244.7 ± 2.6 Ma; Laurent-Charvet et al., 2003).

As mentioned above, the significant strike-slip movements that occurred in late Paleozoic played an important role in the tectonic evolution of the SW CAOB. Such large lateral displacements suggest that the paleogeographic relationships between different tectonic units in the SW CAOB should be totally different from their present-day situations. Thus, it is suggested that a great attention should be paid to the significant strike-slip movements in the tectonic and paleogeographic reconstructions of the SW CAOB.

6. Conclusions

A new paleomagnetic study was conducted on the Early Permian volcanic and sedimentary rocks and the Neoproterozoic mafic dikes from the Yili Block. Magnetite and hematite were identified as the principal magnetic remanence carriers of these rocks. The sole reversed magnetic polarity was revealed by demagnetization. The magnetic remanence of only the Early Permian sequences turned out to be primary and that of the mafic dikes is ambiguous. According to the primary magnetic remanence from the Early Permian sequences, the following conclusions are obtained:

1. The first Early Permian paleomagnetic pole for the Yili Block is calculated as 81.5°N, 256.5°E, N = 11, and A_{95} = 10.9°.
2. New quantitative constraints on the late Paleozoic kinematic evolution of the SW CAOB are acquired by comparing this new pole with published ones from the Yili, Tarim, and South Junggar blocks. Between the Yili and Tarim blocks, significant relative movement took place along major strike-slip faults during the Late Carboniferous to Early Permian (580 ± 290 km) and the Early to Late Permian (585 ± 340 km), and the displacement rate increased from the Late Carboniferous to Early Permian (~19.3 ± 9.7 mm/yr) to the Early to Late Permian (~29.3 ± 17.0 mm/yr). There was no significant relative movement between the Yili and South Junggar blocks during the Late Carboniferous to Early Permian, but a significant relative

rotation of 28.3° ± 18.3° in the Late Permian and a lateral displacement of 630 ± 295 km after the Late Permian occurred between these two blocks.

3. The significant strike-slip movements in the SW CAOB in late Paleozoic are confirmed in this study, and more attention should be paid to them when conducting tectonic and paleogeographic reconstructions in this region.

Our result from the Neoproterozoic dikes may indicate a widespread remagnetization in the studied area, which needs to be verified by future works. More well-time constrained paleomagnetic data are needed, especially from the Yili and Junggar blocks after Permian, to improve the understanding of the intracontinental kinematic history of the SW CAOB.

Acknowledgments
Data supporting Figures 6 and 9 are available in Tables S1 and S2, respectively. We thank Ms. Xuzhi Hu, Yongxiang Li, and Xiaoke Qiang for providing laboratory guidance. We also appreciate Ms. Lifeng Ma and Mrs. Xianqing Jing, Yong Zhang, Wenjun Jiao, France Lagroix, Claire Carvallo, and Yohan Guyodo for their help in the laboratory analyses. Many thanks to the Editor, Prof. John Geissman; the Associate Editor, Prof. Augusto Rapalini; and four reviewers, Dr. Bernard Henry and three anonymous, for their constructive comments and suggestions. This study was cosponsored by the National Nature Science Foundation of China (41772225, 41390445, 41172197, and 41222019), the Fundamental Research Funds for the Central Universities, and by the Open Fund of State Key Laboratory for Mineral Deposits Research (ZZKT-201603). Labex VOLTAIRE (ANR-10-LABX-100-01) is appreciated for financing part of research of the first author in France.

References

Allen, M. B., Windley, B. F., & Zhang, C. (1992). Palaeozoic collisional tectonics and magmatism of the Chinese Tien Shan central Asia. *Tectonophysics*, *220*, 89–115. https://doi.org/10.1016/0040-1951(93)90225-9

Andersen, T. (2002). Correction of common lead in U–Pb analyses that do not report 204Pb. *Chemical Geology*, *192*(1-2), 59–79. https://doi.org/10.1016/S0009-2541(02)00195-X

Ankinovitch, S. G. (1962). The lower Paleozoic of the vanadium-rich Central Tien-Shan Basin and of the Central Kazakhstan West Margin, Nauka KazSSR, Alma-Ata, 189 pp. (in Russian).

Avouac, J. P., & Tapponnier, P. (1993). Kinematic model of active deformation in Central Asia. *Geophysical Research Letters*, *20*, 895–898. https://doi.org/10.1029/93GL00128

Bai, Y., Chen, G., Sun, Q., Sun, Y., Li, Y., Dong, Y., & Sun, D. (1985). Late Paleozoic polar wander path for the Tarim platform and its tectonic significance. *Tectonophysics*, *139*(1–2), 145–153.

Bazhenov, M. L., Burtman, V. S., & Dvorova, A. V. (1999). Permian paleomagnetism of the Tien Shan fold belt, Central Asia: Post-collisional rotations and deformation. *Tectonophysics*, *312*(2-4), 303–329. https://doi.org/10.1016/S0040-1951(99)00181-X

Bazhenov, M. L., Chauvin, A., Audibert, M., & Levashova, N. M. (1993). Permian and Triassic paleomagnetism of the southwestern Tien Shan: Timing and mode of tectonic rotations. *Earth and Planetary Science Letters*, *118*(1-4), 195–212. https://doi.org/10.1016/0012-821X(93)90168-9

Bazhenov, M. L., Collins, A. Q., Degtyarev, K. E., Levashova, N. M., Mikolaichuk, A. V., Pavlov, V. E., & Van der Voo, R. (2003). Paleozoic northward drift of the North Tien Shan (Central Asia) as revealed by Ordovician and Carboniferous paleomagnetism. *Tectonophysics*, *366*(1–2), 113–141. https://doi.org/10.1016/s0040-1951(03)00075-1

Reconstruction of the Paleo-Asian Ocean, VSP InternBerzin, N. A., & Dobretsov, N. L. (1993). Geodynamic evolution of Southern Siberia in Late Precambrian-early Paleozoic time (pp. 45–62). Netherlands: Science Publishers.

Black, L. P., & Gulson, B. L. (1978). The age of the Mud Tank carbonatite, Strangways range, Northern Territory. *BMR Journal of Australian Geology and Geophysics*, *3*(3), 227–232.

Burtman, V. S. (1975). Structure geology of Variscan Tien Shan, USSR. *American Journal of Science*, *275-A*, 157–186.

Butler, R. F. (1992). *Paleomagnetism: Magnetic domains to geologic terranes*. Boston: Blackwell Scientific Publications. https://doi.org/10.1111/j.1749-6632.1992.tb26091.x

Charvet, J., Shu, L. S., Laurent-Charvet, S., Wang, B., Faure, M., Cluzel, D., et al. (2011). Palaeozoic tectonic evolution of the Tianshan belt, NW China. *Science China Earth Sciences*, *54*(2), 166–184. https://doi.org/10.1007/s11430-010-4138-1

Chen, B. H., Luo, Z. H., Jia, B. H., Liu, W., Wei, Y., & Han, Y. G. (2007). SHRIMP U-Pb zircon geochronology of igneous rocks from southern margin of the Alataw Mountains, Xinjiang, China. *Acta Petrologica Sinica*, *23*, 1756–1764.

Chen, J. F., Chen, D. G., Li, X. M., & Zhou, T. X. (1994). K-Ar and 40Ar-39Ar geochronology of granite from the Alatao Mountains, Northwest Xinjiang, China. *Acta Petrologica Sinica*, *10*, 184–192.

Chen, Y., Xu, B., Zhan, S., & Li, Y. (2004). First mid-Neoproterozoic paleomagnetic results from the Tarim Basin (NW China) and their geodynamic implications. *Precambrian Research*, *133*(3–4), 271–281. https://doi.org/10.1016/j.precamres.2004.05.002

Chen, Y. B., Hu, A. Q., Zhan, G. X., & Zhang, Q. F. (2000). Zircon U–Pb age of granitic gneiss on Duku highway in western Tianshan of China and its geological implications. *Chinese Science Bulletin*, *45*(7), 649–653. https://doi.org/10.1007/BF02886044

Chen, Y. J., Liu, Y. L., Bao, J. X., Zhang, Z. J., Chen, H. Y., Cai, W. J., & Herb, H. (2004). Isotopic dating for the volcanic rocks of the Aikendaban formation in West Tianshan, China and its tectonic implication. *Kuangwu Yanshi*, *24*, 52–55.

Choulet, F., Chen, Y., Cogné, J. P., Rabillard, A., Wang, B., Lin, W., et al. (2013). First Triassic palaeomagnetic constraints from Junggar (NW China) and their implications for the Mesozoic tectonics in Central Asia. *Journal of Asian Earth Sciences*, *78*, 371–394. https://doi.org/10.1016/j.jseaes.2013.01.023

Choulet, F., Chen, Y., Wang, B., Faure, M., Cluzel, D., Charvet, J., et al. (2011). Late Paleozoic paleogeographic reconstruction of Western Central Asia based upon paleomagnetic data and its geodynamic implications. *Journal of Asian Earth Sciences*, *42*(5), 867–884. https://doi.org/10.1016/j.jseaes.2010.07.011

Choulet, F., Faure, M., Cluzel, D., Chen, Y., Lin, W., Wang, B., & Jahn, B. M. (2012). Architecture and evolution of accretionary orogens in the Altaids collage: The early Paleozoic West Junggar (NW China). *American Journal of Science*, *312*(10), 1098–1145. https://doi.org/10.2475/10.2012.02

Cogné, J. P. (2003). PaleoMac: A Macintosh™ application for treating paleomagnetic data and making plate reconstructions. *Geochemistry, Geophysics, Geosystems*, *4*(1), 1007. https://doi.org/10.1029/2001GC000227

de Jong, K., Wang, B., Faure, M., Shu, L. S., Cluzel, D., Charvet, J., et al. (2009). New 40Ar/39Ar age constraints on the late Palaeozoic tectonic evolution of the western Tianshan (Xinjiang, northwestern China), with emphasis on Permian fluid ingress. *International Journal of Earth Sciences*, *98*(6), 1239–1258. https://doi.org/10.1007/s00531-008-0338-8

Ding, H. F., Ma, D. S., Yao, C. Y., & Shu, L. S. (2009). Sedimentary environment of Ediacaran glacigenic diamictite in Guozigou of Xinjiang, China. *Chinese Science Bulletin*, *54*(18), 3283–3294. https://doi.org/10.1007/s11434-009-0443-5

Dobretsov, N. L., Buslov, M. M., & Vernikovsky, V. A. (2003). Neoproterozoic to early Ordovician evolution of the Paleo-Asian Ocean: Implications to the break-up of Rodinia. *Gondwana Research*, *6*(2), 143–159. https://doi.org/10.1016/s1342-937x(05)70966-7

Driscoll, P. E., & Evans, D. A. D. (2016). Frequency of Proterozoic geomagnetic superchrons. *Earth and Planetary Science Letters*, *437*, 9–14. https://doi.org/10.1016/j.epsl.2015.12.035

Duan, S. G., Zhang, Z. H., Jiang, Z. S., Zhao, J., Zhang, Y. P., Li, F. M., & Tian, J. Q. (2014). Geology, geochemistry, and geochronology of the Dunde iron-zinc ore deposit in western Tianshan, China. *Ore Geology Reviews*, *57*, 441–461. https://doi.org/10.1016/j.oregeorev.2013.08.019

Dunlop, D. J., Özdemir, Ö., & Schmidt, P. W. (1997). Paleomagnetism and paleothermometry of the Sydney Basin 2. Origin of anomalously high unblocking temperatures. *Journal of Geophysical Research*, *102*, 27,285–27,295. https://doi.org/10.1029/97JB02478

Eizenhöfer, P. R., Zhao, G. C., Zhang, J., & Sun, M. (2014). Final closure of the Paleo-Asian Ocean along the Solonker suture zone: Constraints from geochronological and geochemical data of Permian volcanic and sedimentary rocks. *Tectonics*, *33*, 441–463. https://doi.org/10.1002/2013tc003357

Enkin, R. J. (2003). The direction-correction tilt test: An all-purpose tilt/fold test for paleomagnetic studies. *Earth and Planetary Science Letters*, *212*(1–2), 151–166. https://doi.org/10.1016/S0012-821X(03)00238-3

Fang, D. J., Wang, P. Y., Shen, Z. Y., & Tan, X. D. (1998). Paleomagnetic results and Phanerozoic apparent polar wandering path of Tarim block. *Science China Series D*, *41*(Suppl), 105–112.

Fisher, R. (1953). Dispersion on a sphere. *Proceedings of the Royal Society of London A: Mathematical, Physical and Engineering Sciences*, *217*(1130), 295–305. https://doi.org/10.1098/rspa.1953.0064

Gao, J., Klemd, R., Qian, Q., Zhang, X., Li, J. L., Jiang, T., & Yang, Y. Q. (2011). The collision between the Yili and Tarim blocks of the southwestern Altaids: Geochemical and age constraints of a leucogranite dike crosscutting the HP-LT metamorphic belt in the Chinese Tianshan Orogen. *Tectonophysics*, *499*(1–4), 118–131. https://doi.org/10.1016/j.tecto.2011.01.001

Gao, J., Li, M. S., Xiao, W. J., Tang, Y. Q., & He, G. Q. (1998). Paleozoic tectonic evolution of the Tianshan Orogen, northern China. *Tectonophysics*, *287*(1-4), 213–231. https://doi.org/10.1016/S0040-1951(98)80070-X

Gao, J., Long, L. L., Klemd, R., Qian, Q., Liu, D. Y., Xiong, X. M., et al. (2009). Tectonic evolution of the South Tianshan orogen and adjacent regions, NW China: Geochemical and age constraints of granitoid rocks. *International Journal of Earth Sciences*, *98*(6), 1221–1238. https://doi.org/10.1007/s00531-008-0370-8

Gao, J., Long, L. L., Qian, Q., Huang, D. Z., Su, W., & Klemd, R. (2006). South Tianshan: A late Paleozoic or a Triassic orogen. *Acta Petrologica Sinica*, *22*(5), 1049–1061.

Geng, H. Y., Sun, M., Yuan, C., Zhao, G. C., & Xiao, W. J. (2011). Geochemical and geochronological study of early Carboniferous volcanic rocks from the West Junggar: Petrogenesis and tectonic implications. *Journal of Asian Earth Sciences*, *42*(5), 854–866. https://doi.org/10.1016/j.jseaes.2011.01.006

Gilder, S., Zhao, X., Coe, R., Meng, Z., Courtillot, V., & Besse, J. (1996). Paleomagnetism and tectonics of the southern Tarim Basin, northwestern China. *Journal of Geophysical Research*, *101*, 22,015–22,031. https://doi.org/10.1029/96JB01647

Gou, L. L., Zhang, L. F., Zeng, L., & Shen, T. T. (2015). Geochemistry and geochronology of S-type granites and their coeval MP/HT meta-sedimentary rocks in Chinese southwest Tianshan and their tectonic implications. *Journal of Asian Earth Sciences*, *107*, 151–171. https://doi.org/10.1016/j.jseaes.2015.04.020

Han, B. F., He, G. Q., Wang, X. C., & Guo, Z. J. (2011). Late Carboniferous collision between the Tarim and Kazakhstan-Yili terranes in the western segment of the South Tian Shan Orogen, Central Asia, and implications for the northern Xinjiang, western China. *Earth-Science Reviews*, *109*(3-4), 74–93. https://doi.org/10.1016/j.earscirev.2011.09.001

Hankard, F., Cogn, J. P. E., & Kravchinsky, V. (2005). A new Late Cretaceous paleomagnetic pole for the west of Amuria block (Khurmen Uul, Mongolia). *Earth and Planetary Science Letters*, *236*(1-2), 359–373. https://doi.org/10.1016/j.epsl.2005.05.033

Hounslow, M. W., Davydov, V. I., Klootwijk, C. T., & Turner, P. (2004). Magnetostratigraphy of the Carboniferous: A review and future prospects. *Newsletter on Carboniferous Stratigraphy*, *22*, 35–41.

Hu, A. Q., Wei, G. J., Jahn, B. M., Zhang, J. B., Deng, W. F., & Chen, L. L. (2010). Formation of the 0.9 Ga Neoproterozoic granitoids in the Tianshan Orogen, NW China: Constraints from the SHRIMP zircon age determination and its tectonic significance (in Chinese with English abstract). *Geochimica*, *39*(3), 197–212.

Hu, A. Q., Zhang, G. X., & Chen, Y. B. (2006). *Isotope geochronology and geochemistry for major geological events of continental crustal evolution of Xinjiang, China* (in Chinese with English abstract) (pp. 119–161). Beijing: Geological Publishing House.

Jackson, S. E., Pearson, N. J., Griffin, W. L., & Belousova, E. A. (2004). The application of laser ablation-inductively coupled plasma-mass spectrometry to in situ U–Pb zircon geochronology. *Chemical Geology*, *211*(1–2), 47–69. https://doi.org/10.1016/j.chemgeo.2004.06.017

Jahn, B. M. (2004). The Central Asia Orogenic Belt and growth of the continental crust in the Phanerozoic. In J. Malpas et al. (Eds.), *Aspects of the tectonic evolution of China. Geological Society of London, Special Publications, 226*, 73–100. https://doi.org/10.1144/GSL.SP.2004.226.01.05

Jahn, B. M., Wu, F. Y., & Chen, B. (2000). Granitoids of the Central Asian Orogenic Belt and continental growth in the Phanerozic. *GSA Special Papers*, *350*, 181–193. https://doi.org/10.1130/0-8137-2350-7.181

Jiang, Y. D., Sun, M., Kröner, A., Tumurkhuu, D., Long, X. P., Zhao, G. C., et al. (2012). The high-grade Tseel terrane in SW Mongolia: An Early Paleozoic arc system or a Precambrian sliver? *Lithos*, *142-143*, 95–115. https://doi.org/10.1016/j.lithos.2012.02.016

Kheraskova, T. N., Didenko, A. N., Bush, V. A., & Volozh, Y. A. (2003). The Vendian–early Paleozoic history of the continental margin of eastern Paleogondwana, Paleoasian Ocean, and central Asian foldbelt. *Russian Journal of Earth Sciences*, *5*(3), 165–184. https://doi.org/10.2205/2003ES000123

Kirschvink, J. L. (1980). The least squares line and the analysis of paleomagnetic data. *Geophysical Journal International*, *62*(3), 699–718. https://doi.org/10.1111/j.1365-246X.1980.tb02601.x

Kröner, A., Windley, B. F., Badarch, G., Tomurtogoo, O., Jahn, B. M., Gruschka, S., et al. (2007). Accretionary growth and crust formation in the Central Asian Orogenic Belt and comparison with the Arabian-Nubian shield. *Geological Society of America Memoirs*, *200*, 181–209. https://doi.org/10.1130/2007.1200(11)

Laurent-Charvet, S., Charvet, J., Monié, P., & Shu, L. S. (2003). Late Paleozoic strike-slip shear zones in eastern Central Asia (NW China): New structural and geochronological data. *Tectonics*, *22*(2), 1009. https://doi.org/10.1029/2001TC901047

Laurent-Charvet, S., Charvet, J., Shu, L. S., Ma, R. S., & Lu, H. F. (2002). Palaeozoic late collisional strike-slip deformations in Tianshan and Altay, eastern Xinjiang, NW China. *Terra Nova*, *14*(4), 249–256. https://doi.org/10.1046/j.1365-3121.2002.00417.x

Levashova, N. M., Meert, J. G., Gibsher, A. S., Grice, W. C., & Bazhenov, M. L. (2011). The origin of microcontinents in the Central Asian Orogenic Belt: Constraints from paleomagnetism and geochronology. *Precambrian Research*, *185*(1–2), 37–54. https://doi.org/10.1016/j.precamres.2010.12.001

Levashova, N. M., Van der Voo, R., Abrajevitch, A. V., & Bazhenov, M. L. (2009). Paleomagnetism of mid-Paleozoic subduction-related volcanics from the Chingiz range in NE Kazakhstan: The evolving paleogeography of the amalgamating Eurasian composite continent. *Geological Society of America Bulletin*, *121*(3–4), 555–573. https://doi.org/10.1130/b26354.1

Li, N. B., Niu, H. C., Shan, Q., Jiang, Y. H., Zeng, L. J., Yang, W. B., & Pei, Z. J. (2013). Zircon U-Pb geochronology and geochemistry of post-collisional granitic porphyry from Yuantoushan, Nileke, Xinjiang. *Acta Petrologica Sinica*, *29*(10), 3402–3412.
Li, N. B., Niu, H. C., Shan, Q., & Yang, W. B. (2015). Two episodes of late Paleozoic A-type magmatism in the Qunjisayi area, western Tianshan: Petrogenesis and tectonic implications. *Journal of Asian Earth Sciences*, *113*, 238–253. https://doi.org/10.1016/j.jseaes.2014.12.015
Li, X. Y., Xu, X. Y., Sun, J. M., Li, Z. P., Bai, J. K., & Zhang, X. B. (2012). Geochemistry and dating of the hypabyssal granite body in Nilka County of western Tianshan Mountains. *Geological Bulletin of China*, *31*(12), 1939–1948.
Li, Y., Sharps, R., Mcwilliams, M., Li, Y., Li, Q., & Zhang, W. (1991). Late Paleozoic paleomagnetic results from the Junggar block, northwestern China. *Journal of Geophysical Research*, *96*, 16,047–16,060. https://doi.org/10.1029/91JB01619
Li, Y., Sharps, R., Mcwilliams, M., Nur, A., Li, Y., Li, Q., & Zhang, W. (1989). Paleomagnetic results from late Paleozoic dikes from the northwestern Junggar Block, northwestern China. *Earth and Planetary Science Letters*, *94*(1), 123–130.
Li, Y. J., Sun, L. D., Wu, H. R., Wang, G. L., Yang, C. S., & Peng, G. X. (2005). Permo-Carboniferous radiolarians from the Wupata'erkan group, western south Tianshan, Xinjiang, China. *Acta Geologica Sinica (English Edition)*, *79*(1), 16–23.
Li, Y. J., Wang, Z. M., Wu, H. R., Huang, Z. B., Tan, Z. J., & Luo, J. C. (2002). Discovery of radiolarian fossils from the Aiketik group at the western end of the south Tianshan Mountains of China and its implications. *Acta Geologica Sinica*, *76*(2), 146–154. https://doi.org/10.1111/j.1755-6724.2002.tb00081.x
Liu, H. S., Wang, B., Shu, L. S., Jahn, B. m., & Lizuka, Y. (2014). Detrital zircon ages of Proterozoic meta-sedimentary rocks and Paleozoic sedimentary cover of the northern Yili Block: Implications for the tectonics of microcontinents in the Central Asian Orogenic Belt. *Precambrian Research*, *252*, 209–222. https://doi.org/10.1016/j.precamres.2014.07.018
Liu, Z. Q., Han, B. F., Ji, J. Q., & Li, Z. H. (2005). Ages and geochemistry of the post-collisional granitic rocks from eastern Alataw Mountains, Xinjiang, and implications for vertical crustal growth. *Acta Petrologica Sinica*, *21*(3), 623–639.
Long, L. L., Gao, J., Klemd, R., Beier, C., Qian, Q., Zhang, X., et al. (2011). Geochemical and geochronological studies of granitoid rocks from the western Tianshan Orogen: Implications for continental growth in the southwestern Central Asian Orogenic Belt. *Lithos*, *126*(3-4), 321–340. https://doi.org/10.1016/j.lithos.2011.07.015
Ludwig, K. R. (2001). Squid 1.02: A user manual. Berkeley Geochronological Center, special publication 2, Berkeley, 19 pp.
McElhinny, M. W. (1964). Statistical significance of the fold test in palaeomagnetism. *Geophysical Journal International*, *8*(3), 338–340. https://doi.org/10.1111/j.1365-246X.1964.tb06300.x
Meng, Z. (1991). Palaeomagnetic study of upper Palaeozoic erathem along the southwestern margin of Tarim block, China (in Chinese with English abstract). *Acta Sedimentologica Sinica*, *9*, 105–109.
Mossakovsky, A. A., Ruzhentsev, S. V., Samygin, S. G., & Kheraskova, T. N. (1994). Central Asian fold belt: Geodynamic evolution and formation history. *Geotectonics*, *27*(6), 445–474.
Nie, S. Y., Rowley, D. B., Van der Voo, R., & Li, M. S. (1993). Paleomagnetism of late Paleozoic rocks in the Tianshan, northwestern China. *Tectonics*, *12*, 568–579. https://doi.org/10.1029/92TC00657
Nomade, S., Féraud, G., Chen, Y., & Pouclet, A. (2002). Thermal and tectonic evolution of the paleoproterozoic Transamazonian orogen as deduced from 40 Ar/39 Ar and AMS along the Oyapok river (French Quyana). *Precambrian Research*, *114*(1–2), 35–53. https://doi.org/10.1016/S0301-9268(01)00217-0
Roberts, A. P., Chang, L., Rowan, C. J., Horng, C., & Florindo, F. (2011). Magnetic properties of sedimentary greigite (Fe3S4): An update. *Reviews of Geophysics*, *49*, RG1002. https://doi.org/10.1029/2010RG000336
Safonova, I., Seltmann, R., Kröner, A., Gladkochub, D., Schulmann, K., Xiao, W. J., et al. (2011). A new concept of continental construction in the Central Asian Orogenic Belt (compared to actualistic examples from the Western Pacific). *Episodes*, *34*(3), 186–196.
Sengör, A. M. C., & Natal'in, B. A. (1996). Paleotectonics of Asia: fragments of a synthesis. In A. Yin & M. Harrison (Eds.), *The Tectonic Evolution of Asia* (pp. 486–640). Cambridge: Cambridge University Press.
Sengör, A. M. C., Natal'in, B. A., & Burtman, V. S. (1993). Evolution of the Altaid tectonic collage and Palaeozoic crustal growth in Eurasia. *Nature*, *364*(6435), 299–307. https://doi.org/10.1038/364299a0
Sharps, R., Li, Y. P., McWilliams, M., & Li, Y. G. (1992). Paleomagnetic investigation of Upper Permian sediments in the south Junggar Basin, China. *Journal of Geophysical Research*, *97*, 1753–1765. https://doi.org/10.1029/91JB02741
Sharps, R., Mcwilliams, M., Li, Y., Cox, A., Zhang, Z., Zhai, Y., et al. (1989). Lower Permian paleomagnetism of the Tarim block, northwestern China. *Earth and Planetary Science Letters*, *92*(3–4), 275–291. https://doi.org/10.1016/0012-821X(89)90052-6
Shu, L. S., Charvet, J., Lu, H. F., & Laurent-Charvet, S. (2002). Paleozoic accretion-collision events and kinematics of ductile deformation in the central-southern Tianshan Belt, China. *Acta Geologica Sinica (English Edition)*, *76*(3), 308–323.
Shu, L. S., Deng, X. L., Zhu, W. B., Ma, D. S., & Xiao, W. J. (2011). Precambrian tectonic evolution of the Tarim Block, NW China: New geochronological insights from the Quruqtagh domain. *Journal of Asian Earth Sciences*, *42*(5), 774–790. https://doi.org/10.1016/j.jseaes.2010.08.018
Shu, L. S., Yu, J. H., Charvet, J., Laurent-Charvet, S., Sang, H. Q., & Zhang, R. G. (2004). Geological, geochronological and geochemical features of granulites in the eastern Tianshan, NW China. *Journal of Asian Earth Sciences*, *24*(1), 25–41. https://doi.org/10.1016/j.jseaes.2003.07.002
Silva, P. F., Henry, B., Marques, F. O., Madureira, P., & Miranda, J. M. (2006). Paleomagnetic study of the Great Foum Zguid dyke (southern Morocco): A positive contact test related to metasomatic processes. *Geophysical Research Letters*, *33*, L21301. https://doi.org/10.1029/2006GL027498
Tang, G. J., Wang, Q., Wyman, D. A., Sun, M., Li, Z. X., Zhao, Z. H., et al. (2010). Geochronology and geochemistry of late Paleozoic magmatic rocks in the Lamasu-Dabate area, northwestern Tianshan (West China): Evidence for a tectonic transition from arc to post-collisional setting. *Lithos*, *119*(3–4), 393–411. https://doi.org/10.1016/j.lithos.2010.07.010
Tauxe, L., Butler, R. F., Van, d. V. R., & Banerjee, S. K. (2010). *Essentials of paleomagnetism*. Berkeley, CA: University of California Press. https://doi.org/10.1016/j.ijfoodmicro.2009.10.014
Voo, R. V. D. (1993). *Paleomagnetism of the Atlantic, Tethys and Iapetus Oceans*. Cambridge, UK: Cambridge: Cambridge University Press.
Wang, B., Chen, Y., Zhan, S., Shu, L. S., Faure, M., Cluzel, D., et al. (2007). Primary Carboniferous and Permian paleomagnetic results from the Yili Block (NW China) and their implications on the geodynamic evolution of Chinese Tianshan Belt. *Earth and Planetary Science Letters*, *263*(3–4), 288–308. https://doi.org/10.1016/j.epsl.2007.08.037
Wang, B., Cluzel, D., Shu, L., Faure, M., Charvet, J., Chen, Y., et al. (2009). Evolution of calc-alkaline to alkaline magmatism through Carboniferous convergence to Permian transcurrent tectonics, western Chinese Tianshan. *International Journal of Earth Sciences*, *98*(6), 1275–1298. https://doi.org/10.1007/s00531-008-0408-y
Wang, B., Faure, M., Cluzel, D., Shu, L. S., Charvet, J., Meffre, S., & Ma, Q. (2006). Late Paleozoic tectonic evolution of the northern west Chinese Tianshan Belt. *Geodinamica Acta*, *19*(3–4), 237–247. https://doi.org/10.3166/ga.19.237-247

Wang, B., Faure, M., Shu, L. S., Cluzel, D., Charvet, J., de Jong, K., & Chen, Y. (2008). Paleozoic geodynamic evolution of the Yili Block, western Chinese Tianshan. *Bulletin de la Société Géologique de France*, *179*(5), 483–490. https://doi.org/10.2113/gssgfbull.179.5.483

Wang, B., Faure, M., Shu, L. S., de Jong, K., Charvet, J., Cluzel, D., et al. (2010). Structural and geochronological study of high-pressure metamorphic rocks in the Kekesu section (northwestern China): Implications for the late Paleozoic tectonics of the southern Tianshan. *The Journal of Geology*, *118*(1), 59–77. https://doi.org/10.1086/648531

Wang, B., Jahn, B. M., Lo, C. H., Shu, L. S., Wu, C., Li, K., & Wang, F. (2011). Structural analysis and 40Ar/39Ar thermochronology of Proterozoic rocks in Sailimu area (NW China): Implication to polyphase tectonics of the North Chinese Tianshan. *Journal of Asian Earth Sciences*, *42*(5), 839–853. https://doi.org/10.1016/j.jseaes.2011.07.022

Wang, B., Jahn, B. M., Shu, L. S., Li, K. S., Chung, S., & Liu, D. Y. (2012). Middle-late Ordovician arc-type plutonism in the NW Chinese Tianshan: Implication for the accretion of the Kazakhstan continent in Central Asia. *Journal of Asian Earth Sciences*, *49*, 40–53. https://doi.org/10.1016/j.jseaes.2011.11.005

Wang, B., Liu, H. S., Shu, L. S., Jahn, B. m., Chung, S., Zhai, Y. Z., and Liu, D. Y. (2014). Early Neoproterozoic crustal evolution in northern Yili Block: Insights from migmatite, orthogneiss and leucogranite of the Wenquan metamorphic complex in the NW Chinese Tianshan. *Precambrian Research*, *242*, 58–81. https://doi.org/10.1016/j.precamres.2013.12.006

Wang, B., Shu, L. S., Cluzel, D., Faure, M., & Charvet, J. (2007). Geochronological and geochemical studies on the Borohoro plutons, north of Yili, NW Tianshan and their tectonic implication. *Acta Petrologica Sinica*, *8*, 1885–1900.

Wang, B., Shu, L. S., Faure, M., Jahn, B. m., Cluzel, D., Charvet, J., et al. (2011). Paleozoic tectonics of the southern Chinese Tianshan: Insights from structural, chronological and geochemical studies of the Heiyingshan ophiolitic mélange (NW China). *Tectonophysics*, *497*(1–4), 85–104. https://doi.org/10.1016/j.tecto.2010.11.004

Wang, B., Shu, L. S., Liu, H. S., Gong, H. J., Ma, Y. Z., Mu, L. X., & Zhong, L. L. (2014). First evidence for ca. 780Ma intra-plate magmatism and its implications for Neoproterozoic rifting of the north Yili Block and tectonic origin of the continental blocks in SW of Central Asia. *Precambrian Research*, *254*, 258–272. https://doi.org/10.1016/j.precamres.2014.09.005

Wang, B., Zhai, Y. Z., Kapp, P., de Jong, K., Liu, H. S., Zhong, L. L., et al. (2018). Accretionary tectonics of back-arc oceanic basins in the south Tianshan: Insights from structural, geochronological and geochemical studies of the Wuwamen ophiolite mélange. *Bulletin Geological Society of America*, *130*(1–2), 284–306. https://doi.org/10.1130/B31397.1

Wang, Z. L., Mao, J. W., Yang, J. M., Han, C. M., Chen, W., & Zhang, Z. H. (2004). 40Ar-39Ar isotope dating of K-feldspar from moyite in the Qiaohuote copper deposit, Xinjiang, and its geological implication. *Acta Petrologica et Mineralogica*, *23*(1), 12–18.

Wen, B., Li, Y. X., & Zhu, W. B. (2013). Paleomagnetism of the Neoproterozoic diamictites of the Qiaoenbrak formation in the Aksu area, NW China: Constraints on the paleogeographic position of the Tarim Block. *Precambrian Research*, *226*, 75–90. https://doi.org/10.1016/j.precamres.2012.10.018

Wilhem, C., Windley, B. F., & Stampfli, G. M. (2012). The Altaids of Central Asia: A tectonic and evolutionary innovative review. *Earth-Science Reviews*, *113*(3–4), 303–341. https://doi.org/10.1016/j.earscirev.2012.04.001

Windley, B. F., Alexeiev, D., Xiao, W. J., Kröner, A., & Badarch, G. (2007). Tectonic models for accretion of the Central Asian Orogenic Belt. *Journal of the Geological Society*, *164*(1), 31–47. https://doi.org/10.1144/0016-76492006-022

Wong, K., Sun, M., Zhao, G. C., Yuan, C., & Xiao, W. J. (2010). Geochemical and geochronological studies of the Alegedayi Ophiolitic Complex and its implication for the evolution of the Chinese Altai. *Gondwana Research*, *18*(2–3), 438–454. https://doi.org/10.1016/j.gr.2010.01.010

XBGMR (Xinjiang Bureau of Geology and Mineral Resources) (1988a). Geological map 1:200000, Baskan Pass-Huocheng Sheet (L-44-26, 27 and 28).

XBGMR (Xinjiang Bureau of Geology and Mineral Resources) (1988b). Geological map 1:200000, Sailimu Sheet (L-44-34).

XBGMR (Xinjiang Bureau of Geology and Mineral Resources) (1993). Regional geology of Xinjiang Uygur autonomy region. Geology Publishing House, Beijing, 1–841 (in Chinese with English abstract).

Xiao, W. J., Han, C. M., Yuan, C., Sun, M., Lin, S. F., Chen, H. L., et al. (2008). Middle Cambrian to Permian subduction-related accretionary orogenesis of northern Xinjiang, NW China: Implications for the tectonic evolution of Central Asia. *Journal of Asian Earth Sciences*, *32*(2–4), 102–117. https://doi.org/10.1016/j.jseaes.2007.10.008

Xiao, W. J., Huang, B. C., Han, C. M., Sun, S., & Li, J. L. (2010). A review of the western part of the Altaids: A key to understanding the architecture of accretionary orogens. *Gondwana Research*, *18*(2–3), 253–273. https://doi.org/10.1016/j.gr.2010.01.007

Xiao, W. J., Windley, B. F., Allen, M. B., & Han, C. M. (2013). Paleozoic multiple accretionary and collisional tectonics of the Chinese Tianshan orogenic collage. *Gondwana Research*, *23*(4), 1316–1341. https://doi.org/10.1016/j.gr.2012.01.012

Xiao, W. J., Windley, B. F., Badarch, G., Sun, S., Li, J., Qin, K., & Wang, Z. (2004). Paleozoic accretionary and convergent tectonics of the southern Altaids: Implications for the lateral growth of Central Asia. *Journal of Geological Society*, *161*(3), 339–342. https://doi.org/10.1144/0016-764903-165

Xiao, W. J., Windley, B. F., Sun, S., Li, J. L., Huang, B. C., Han, C. M., et al. (2015). A tale of amalgamation of three Permo-Triassic Collage Systems in Central Asia: Oroclines, sutures, and terminal accretion. *Annual Review of Earth and Planetary Sciences*, *43*(1), 477–507. https://doi.org/10.1146/annurev-earth-060614-105254

Xu, X. Y., Ma, Z. P., Xia, Z. C., Xia, L. Q., Li, X. M., & Wang, L. S. (2006). TIMS U-Pb isotopic dating and geochemical characteristics of Paleozoic granitic rocks from the middle-western section of Tianshan. *Northwestern Geology*, *39*(1), 50–75.

Xu, X. Y., Wang, H. L., Li, P., Chen, J. L., Ma, Z. P., Zhu, T., et al. (2013). Geochemistry and geochronology of Paleozoic intrusions in the Nalati (Narati) area in western Tianshan, Xinjiang, China: Implications for Paleozoic tectonic evolution. *Journal of Asian Earth Sciences*, *72*, 33–62. https://doi.org/10.1016/j.jseaes.2012.11.023

Yang, W. B., Niu, H. C., Shan, Q., Luo, Y., Sun, W. D., Li, C. Y., et al. (2012). Late Paleozoic calc-alkaline to shoshonitic magmatism and its geodynamic implications, Yuximolegai area, western Tianshan, Xinjiang. *Gondwana Research*, *22*(1), 325–340. https://doi.org/10.1016/j.gr.2011.10.008

Yin, A., & Nie, S. Y. (1996). A Phanerozoic palinspastic reconstruction of China and its neighboring regions. In A. Yin, & M. Harrison (Eds.), *The tectonic evolution of Asia, Rubey Colloquium*, (pp. 442–485). Cambridge: Cambridge University Press.

Yin, J. Y., Yuan, C., Sun, M., Long, X. P., Zhao, G. C., Wong, K. P., et al. (2010). Late Carboniferous high-Mg dioritic dikes in western Junggar, NW China: Geochemical features, petrogenesis and tectonic implications. *Gondwana Research*, *17*(1), 145–152. https://doi.org/10.1016/j.gr.2009.05.011

Zhan, S., Chen, Y., Xu, B., Wang, B., & Faure, M. (2007). Late Neoproterozoic paleomagnetic results from the Sugetbrak formation of the Aksu area, Tarim basin (NW China) and their implications to paleogeographic reconstructions and the snowball Earth hypothesis. *Precambrian Research*, *154*(3–4), 143–158. https://doi.org/10.1016/j.precamres.2007.01.001

Zhang, D. Y., Zhang, Z. C., Encarnación, J., Xue, C. J., Duan, S. G., Zhao, Z. D., & Liu, J. L. (2012). Petrogenesis of the Kekesai composite intrusion, western Tianshan, NW China: Implications for tectonic evolution during late Paleozoic time. *Lithos*, *146*, 65–79. https://doi.org/10.1016/j.lithos.2012.04.002

Zhang, X., Tian, J. Q., Gao, J., Klemd, R., Dong, L. H., Fan, J. J., et al. (2012). Geochronology and geochemistry of granitoid rocks from the Zhibo syngenetic volcanogenic iron ore deposit in the western Tianshan Mountains (NW-China): Constraints on the age of mineralization and tectonic setting. *Gondwana Research*, *22*(2), 585–596. https://doi.org/10.1016/j.gr.2011.06.007

Zhang, Z. H., Wang, Z. L., Zuo, G. C., Liu, M., Wang, L. S., & Wang, J. W. (2008). Ages and tectonic settings of the volcanic rocks in Dabate ore district in west Tianshan Mountains and their constraints on the porphyry-type mineralization. *Acta Petrologica Sinica*, *82*, 1494–1503.

Zhao, J. M., Liu, G. D., Lu, Z. X., Zhang, X. K., & Zhao, G. Z. (2003). Lithospheric structure and dynamic processes of the Tianshan orogenic belt and the Junggar basin. *Tectonophysics*, *376*(3–4), 199–239. https://doi.org/10.1016/j.tecto.2003.07.001

Zhao, P., Chen, Y., Zhan, S., Xu, B., & Faure, M. (2014). The apparent polar wander path of the Tarim block (NW China) since the Neoproterozoic and its implications for a long-term Tarim-Australia connection. *Precambrian Research*, *242*, 39–57. https://doi.org/10.1016/j.precamres.2013.12.009

Zhao, Z. H., Bai, Z. H., Xiong, X. L., Mei, H. J., & Wang, Y. X. (2003). $^{40}Ar/^{39}Ar$ chronological study of late Paleozoic volcanic-hypabyssal igneous rocks in western Tianshan, Xinjiang. *Geochimica*, *32*(4), 317–327.

Zhou, D., Graham, S. A., Chang, E. Z., Wang, B. Y., & Hacker, B. (2001). Paleozoic tectonic amalgamation of the Chinese Tianshan: Evidence from a transect along the Dushanzi-Kuqa highway. In M. S. Hendrix & G. A. Davis (Eds.), *Paleozoic and Mesozoic tectonic evolution of Central Asia: From continental assembly to intracontinental deformation, Boulder, Colorado. Memoirs-Geological Society of America*, *194*, 23–46. https://doi.org/10.1130/0-8137-1194-0.23

Zijderveld, J. D. A. (1967). A.C. demagnetization of rocks: Analysis of results. In D. W. Collinson, K. M. Creer, & S. K. Runcorn (Eds.), *Methods on paleomagnetism* (pp. 245–286). New York: Elsevier.